J|A|C|S
ARTICLES
Published on Web 11/01/2006

$AlMe_3$ and $ZnMe_2$ Adducts of a Titanium Imido Methyl Cation: A Combined Crystallographic, Spectroscopic, and DFT Study

Paul D. Bolton,[†] Eric Clot,*[,‡] Andrew R. Cowley,[†] and Philip Mountford*[,†]

Contribution from the Chemistry Research Laboratory, University of Oxford, Mansfield Road, Oxford OX1 3TA, U.K., and Laboratoire de Structure et Dynamique des Systèmes Moléculaires et Solides (UMR 5636 CNRS-UM2), Université Montpellier 2, Institut Charles Gerhardt, cc 14, 34095 Montpellier Cedex 5, France

Received August 3, 2006; E-mail: philip.mountford@chem.ox.ac.uk

Abstract: A combined experimental and DFT study of the reactions of the titanium imido methyl cation $[Ti(N^tBu)(Me_3[9]aneN_3)Me]^+$ (**4**$^+$) with $AlMe_3$ and $ZnMe_2$ is described. Reaction of **4**$^+$ with $AlMe_3$ gave $[Ti(N^tBu)(Me_3[9]aneN_3)(\mu\text{-}Me)_2AlMe_2]^+$ (**7**$^+$), the first structurally characterized $AlMe_3$ adduct of a transition metal alkyl cation and a model for the presumed resting state in MAO-activated olefin polymerizations. Reaction of **4**$^+$ with $ZnMe_2$ also gave a methyl-bridged heterobinuclear species, namely $[Ti(\mu\text{-}N^tBu)(Me_3[9]aneN_3)(\mu\text{-}Me)_2ZnMe]^+$ (**8**$^+$), the first directly observed $ZnMe_2$ adduct of a transition metal alkyl cation. At room temperature, all three metal-bound methyls of **8**$^+$ underwent rapid exchange with those of free $ZnMe_2$, whereas at 233 K only the terminal Zn−Me group exchanged significantly. Addition of $AlMe_3$ to **8**$^+$ quantitatively formed **7**$^+$ and $ZnMe_2$. Reaction of **4**$^+$ with Cp_2ZrMe_2 gave $[Ti(N^tBu)\{Me_2(\mu\text{-}CH_2)[9]aneN_3\}(\mu\text{-}CH_2)ZrCp_2]^+$ (**10**$^+$) via a highly selective double C−H bond activation reaction in which both alkyl groups of Cp_2ZrMe_2 were lost. DFT calculations on models of **7**$^+$ confirmed the approximately square-based pyramidal geometries for the bridging methyl groups. Calculations on **8**$^+$ found that the formation of the $Ti(\mu\text{-}Me)_2Zn$ moiety is assisted by an $N_{imide}\rightarrow Zn$ dative bond. DFT calculations for the sterically less encumbered methyl cation $[Ti(NMe)(H_3[9]aneN_3)Me]^+$ found strong thermodynamic preferences for adducts featuring $N_{imide}\rightarrow M$ (M = Al or Zn) interactions. This offers insight into recently observed structure−productivity trends in MAO-activated imido-based polymerization catalysts. Calculations on the metallocenium adducts $[Cp_2Ti(\mu\text{-}Me)_2AlMe_2]^+$ and $[Cp_2Ti(\mu\text{-}Me)_2ZnMe]^+$ are described, each showing α-agostic interactions for the bridging methyl groups. For these systems and the imido ones, the coordination of $AlMe_3$ to the corresponding monomethyl cation is ca. 30 kJ mol^{-1} more favorable than for $ZnMe_2$.

Introduction

Olefin polymerization catalysis continues to be an area of considerable importance to both the academic and industrial communities, and a wide range of cyclopentadienyl- and non-cyclopentadienyl-based systems have been described.[1−11] Cationic alkyl complexes "$[L_nM-R]^+$" are accepted as being the active species in Ziegler−Natta type olefin polymerization catalysis.[2,4,5,8] However, in systems activated by MAO (which typically contains up to 15 wt % Al_2Me_6 (hereafter referred to as "$AlMe_3$")) the catalyst resting state is probably a cationic bimetallic species of the type $[L_nM(\mu\text{-}R)_2AlR_2]^+$. A number of such cationic group 4 heterobimetallic cations have been studied spectroscopically during the last 10 years.[12−21] Intermediates of the type $[L_nM(\mu\text{-}R)_2AlR_2]^+$ are known to be important in chain transfer (to aluminum) and catalyst deactivation in olefin polymerization catalyst systems.[5] Gibson has correlated chain transfer to aluminum with the presence of bimetallic complexes

[†] University of Oxford.
[‡] Institut Charles Gerhardt.

(1) Bochmann, M. *J. Chem. Soc., Dalton Trans.* **1996**, 255.
(2) Brintzinger, H. H.; Fischer, D.; Mülhaupt, R.; Rieger, B.; Waymouth, R. M. *Angew. Chem., Int. Ed. Engl.* **1995**, *34*, 1143.
(3) Janiak, C. In *Metallocenes: synthesis, reactivity, applications*; Togni, A., Halterman, R. L., Eds.; Wiley-VCH: New York, 1998; Vol. 2, p 547.
(4) Kaminsky, W. *J. Chem. Soc., Dalton Trans.* **1998**, 1413.
(5) Bochmann, M. *J. Organomet. Chem.* **2004**, *689*, 3982.
(6) McKnight, A. L.; Waymouth, R. M. *Chem. Rev.* **1998**, *98*, 2587.
(7) Britovsek, G. J. P.; Gibson, V. C.; Wass, D. F. *Angew. Chem., Int. Ed.* **1999**, *38*, 429.
(8) Gibson, V. C.; Spitzmesser, S. K. *Chem. Rev.* **2003**, *103*, 283.
(9) Suzuki, Y.; Terao, H.; Fujita, T. *Bull. Chem. Soc. Jpn.* **2003**, *76*, 1493.
(10) Mitani, M.; Saito, J.; Ishii, S.; Nakayama, Y.; Makio, H.; Matsukawa, N.; Matsui, S.; Mohri, J.; Furuyama, R.; Terao, H.; Bando, H.; H., T.; Fujita, T. *Chem. Rec.* **2004**, *4*, 137.
(11) Bolton, P. D.; Mountford, P. *Adv. Synth. Catal.* **2005**, *347*, 355.
(12) Bochmann, M.; Lancaster, S. J. *Angew. Chem., Int. Ed. Engl.* **1994**, *33*, 1634.
(13) Bochmann, M.; Lancaster, S. J. *J. Organomet. Chem.* **1995**, *497*, 55.
(14) Tritto, I.; Donetti, R.; Sacchi, M. C.; Locatelli, P.; Zannoni, G. *Macromolecules* **1997**, *30*, 1247.
(15) Vollmerhaus, R.; Rahim, M.; Tomaszewski, R.; Xin, S.; Taylor, N. J.; Collins, S. *Organometallics* **2000**, *19*, 2161.
(16) Zakharov, I. I.; Zakharov, V. A. *Macromol. Theory Simul.* **2002**, *11*, 352.
(17) Bryliakov, K. P.; Talsi, E. P.; Bochmann, M. *Organometallics* **2004**, *23*, 149.
(18) Schröder, L.; Brintzinger, H. H.; Babushkin, D. E.; Fischer, D.; Mülhaupt, R. *Organometallics* **2005**, *24*, 867.
(19) Bryliakov, K. P.; Babushkin, D. E.; Talsi, E. P.; Voskobynikov, A. Z.; Gritzo, H.; Schröder, L.; Damrau, H.-R. H.; Wieser, U.; Schaper, F.; Brintzinger, H. H. *Organometallics* **2005**, *24*, 894.
(20) Petros, R. A.; Norton, J. R. *Organometallics* **2005**, *23*, 5105.
(21) Eilertsen, J. L.; Støvneng, J. A.; Ystenes, M.; Rytter, E. *Inorg. Chem.* **2005**, *44*, 4843.

$[L_nM(\mu\text{-}R)_2AlR_2]^{n+}$ as catalyst resting states.[22] Remarkably, although neutral rare earth compounds containing coordinated $AlMe_4$ groups have been crystallographically characterized,[23−31] no structural data are available on the nature of the $M(\mu\text{-}R)_2AlR_2$ moiety for transition metals (the bonding in which can be expected to differ from that in rare earth systems).

Dialkyl zinc compounds also play an important role in olefin polymerization, for example to control molecular weight by chain transfer to zinc.[32] Brintzinger has reported the influence of added aluminum and zinc alkyls on the polymerization characteristics of cationic *ansa*-zirconocene catalyst systems,[33] and it was concluded that zinc alkyls (even more so than certain aluminum alkyls) influence productivity and chain transfer through the formation of cationic heterobimetallic adducts. In a variant of the chain transfer process, reports have appeared on the ability of transition metal polymerization catalysts to promote polyethylene chain growth on zinc.[22,34] This occurs through rapid and reversible polymeryl/alkyl group exchange processes between a cationic transition metal species and zinc. In this context, it has been proposed that dialkyl zinc adducts of transition metal alkyl cations (of the type $[L_nM(\mu\text{-}R)_2ZnR]^+$) are thermodynamically less stable than the corresponding $AlMe_3$ adducts. However, no direct experimental observation or computational study has yet tested this. Very recently, $ZnEt_2$ has been used as a "chain shuttling agent" in the highly novel and commercially important catalytic production of olefin block copolymers.[35] Polymeryl-bridged transition metal/zinc heterobimetallic species were again proposed as intermediates in this system.

Many transition metal imido compounds ($L_nM{=}NR$) have also been shown to act as olefin polymerization precatalysts.[11] We recently reported that compounds of the type **1-R** and **2-R** (Figure 1), containing either a $Me_3[9]aneN_3$ (1,4,7-trimethyltriazacyclononane)[36,37] or tris(3,5-dimethylpyrazolyl)methane[38] coligand, form very highly active ethylene homopolymerization catalysts on activation with MAO (methyl aluminoxanes). The precatalyst families **1-R** and **2-R** are isolobal analogues of the ubiquitous group 4 metallocenes Cp_2MCl_2.[39] It was consistently found that only compounds containing a bulky imido N-substituent formed active and robust catalysts, implying that adequate steric protection of the Ti═NR bond is an absolute prerequisite for highly active systems. In the case of the **1-R**/MAO and **2-R**/MAO catalyst systems, several direct observations suggest an important role for $AlMe_3$.[36,37] In particular, addition of 2,6-di-*tert*-butyl-*p*-cresol, a proven $AlMe_3$ scavenger,[40,41] to the $Ti(N^tBu)(Me_3[9]aneN_3)Cl_2$/MAO catalyst system led to higher productivities, higher M_n values and more chain end unsaturations.[37]

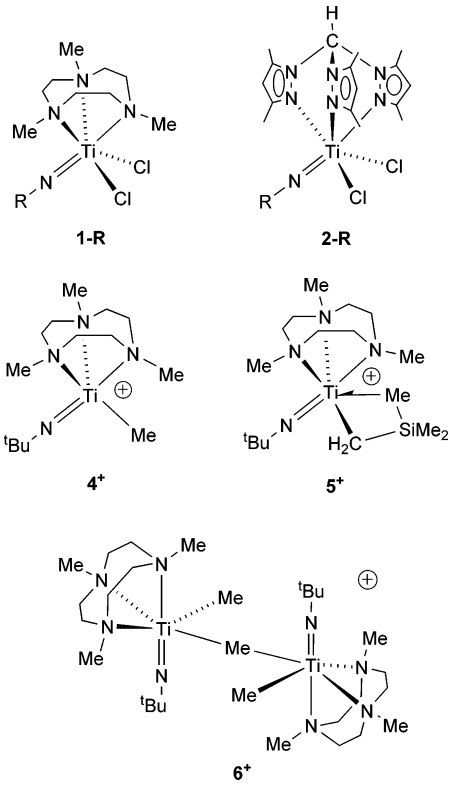

Figure 1. Imido-supported polymerization catalysts and well-defined mono- and binuclear alkyl cations.[36−39]

We recently showed that treatment of $Ti(N^tBu)(Me_3[9]aneN_3)R_2$ (R = Me (**3**) or CH_2SiMe_3) with $[CPh_3]^+$ formed the 14 valence electron cations $[Ti(N^tBu)(Me_3[9]aneN_3)R]^+$ (R = Me ($\mathbf{4}^+$) or CH_2SiMe_3 ($\mathbf{5}^+$); Figure 1).[39] Although they are too reactive to be isolated (except as Lewis base adducts), cations $\mathbf{4}^+$ and/or $\mathbf{5}^+$ can nonetheless readily be generated in situ and used in further reactions, for example in a C−H bond activation of pyridine, stoichiometric Ti−R bond migratory insertion reactions with unsaturated substrates, and formation of the μ-methyl-bridged cation $[Ti_2(N^tBu)_2(Me_3[9]aneN_3)_2Me_2(\mu\text{-}Me)]^+$ ($\mathbf{6}^+$, Figure 1) with $Ti(N^tBu)(Me_3[9]aneN_3)Me_2$.[39,42] The ready access to $\mathbf{4}^+$ offered an excellent opportunity to probe the type(s) of $AlMe_3$ adduct formed in the **1-R**/MAO catalyst systems and also to carry out related studies.

(22) Britovsek, G. J. P.; Cohen, S. A.; Gibson, V. C.; van Meurs, M. *J. Am. Chem. Soc.* **2004**, *126*, 10701.
(23) Holton, J.; Lappert, M. F.; Scollary, G. R.; Ballard, D. G. H.; Pearce, R.; Atwood, J. L.; Hunter, W. E. *J. Chem. Soc., Chem. Commun.* **1976**, 425.
(24) Evans, W. J.; Anwander, R.; Ziller, J. W. *Organometallics* **1995**, *14*, 1107.
(25) Klooster, W. T.; Lu, R. S.; Anwander, R.; Evans, W. J.; Koetzle, T. F.; Bau, R. *Angew. Chem., Int. Ed.* **1998**, *37*, 1268.
(26) Klimpel, M. G.; Anwander, R.; Tafipolsky, M.; Scherer, W. *Organometallics* **2001**, *20*, 3983.
(27) Klimpel, M. G.; Eppinger, J.; Sirsch, P.; Scherer, W.; Anwander, R. *Organometallics* **2002**, *21*, 4021.
(28) Giesbrecht, G. R.; Gordon, J. C.; Brady, J. T.; Clark, D. L.; Keogh, D. W.; Michalczyk, R.; Scott, B. L.; Watkin, J. G. *Eur. J. Inorg. Chem.* **2002**, 723.
(29) Gordon, J. C.; Giesbrecht, G. R.; Brady, J. T.; Clark, D. L.; Keogh, D. W.; Scott, B. L.; Watkin, J. G. *Organometallics* **2002**, *21*, 127.
(30) Anwander, R.; Klimpel, M. G.; Dietrich, H. M.; Shorokhov, D. J.; Scherer, W. *Chem. Commun.* **2003**, 1008.
(31) Fischbach, A.; Herdtweck, E.; Anwander, R.; Eickerling, G.; Scherer, W. *Organometallics* **2003**, 499.
(32) For leading citations, see refs 22 and 33−35.
(33) Bhriain, N. N.; Brintzinger, H. H.; Ruchatz, D.; Fink, G. *Macromolecules* **2005**, *38*, 2056.
(34) van Meurs, M.; Britovsek, G. J. P.; Gibson, V. C.; Cohen, S. A. *J. Am. Chem. Soc.* **2005**, *127*, 9913.
(35) Arriola, D. J.; Carnahan, E. M.; Hustad, P. D.; Kuhlman, R. L.; Wenzel, T. T. *Science* **2006**, *312*, 714.
(36) Adams, N.; Arts, H. J.; Bolton, P. D.; Cowell, D.; Dubberley, S. R.; Friederichs, N.; Grant, C.; Kranenburg, M.; Sealey, A. J.; Wang, B.; Wilson, P. J.; Cowley, A. R.; Mountford, P.; Schröder, M. *Chem. Commun.* **2004**, 434.
(37) Adams, N.; Arts, H. J.; Bolton, P. D.; Cowell, D.; Dubberley, S. R.; Friederichs, N.; Grant, C. M.; Kranenburg, M.; Sealey, A. J.; Wang, B.; Wilson, P. J.; Zuideveld, M. A.; Blake, A. J.; Schröder, M.; Mountford, P. *Organometallics* **2006**, *25*, 3888.
(38) Bigmore, H. R.; Dubberley, S. R.; Kranenburg, M.; Lawrence, S. C.; Sealey, A. J.; Selby, J. D.; Zuideveld, M.; Cowley, A. R.; Mountford, P. *Chem. Commun.* **2006**, 436.
(39) Bolton, P. D.; Clot, E.; Adams, N.; Dubberley, S. R.; Cowley, A. R.; Mountford, P. *Organometallics* **2006**, *25*, 2806.
(40) Williams, V. C.; Dai, C.; Li, Z.; Collins, S.; Piers, W. E.; Clegg, W.; Elsegood, M. R. J.; Marder, T. B. *Angew. Chem., Int. Ed.* **1999**, *38*, 3695.
(41) Busico, V.; Cipullo, R.; Cutillo, F.; Friederichs, N.; Ronca, S.; Wang, B. *J. Am. Chem. Soc.* **2003**, *125*, 12402.
(42) Bolton, P. D.; Clot, E.; Cowley, A. R.; Mountford, P. *Chem. Commun.* **2005**, 3313.

Scheme 1. Synthesis of Cationic Heterobimetallic Complexes[a]

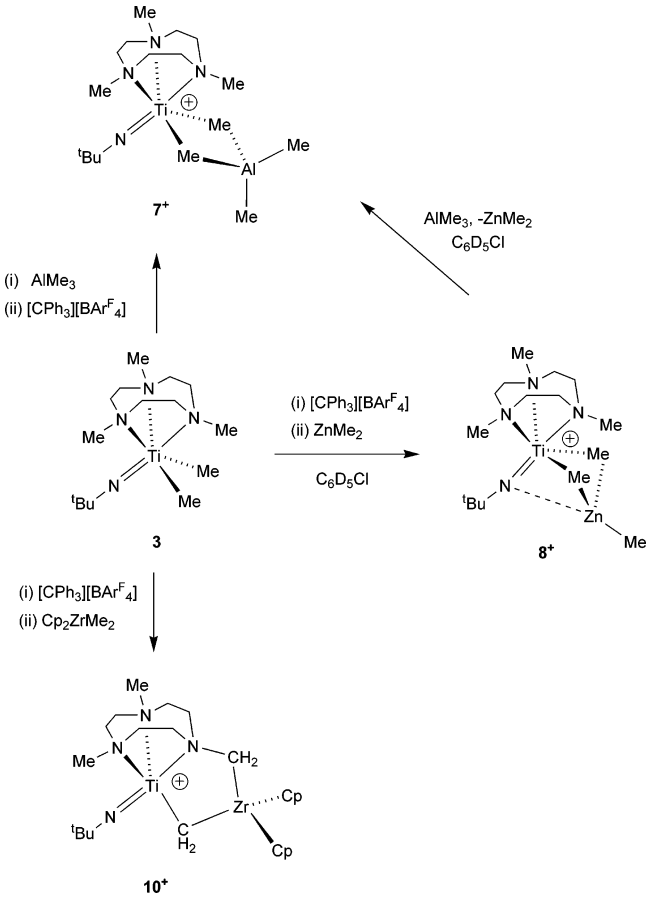

[a] Anions are omitted for clarity.

In this contribution we describe the reaction of $\mathbf{4}^+$ with $AlMe_3$, together with complimentary studies for $ZnMe_2$ and Cp_2ZrMe_2. In addition, a comprehensive DFT study of a selection of both real and hypothetical adducts formed with the two main group alkyls is described. These combined experimental and DFT studies provide valuable insight into the molecular and electronic structures and energetic aspects of $AlMe_3$ and $ZnMe_2$ adducts of group 4 monomethyl cations. A part of this work (namely the synthesis and characterization of [Ti(N^{t}Bu)(Me$_3$[9]aneN$_3$)(μ-Me)$_2$AlMe$_2$][BAr$^F_4$]) has been communicated.[42]

Results and Discussion

Reaction of [Ti(N^{t}Bu)(Me$_3$[9]aneN$_3$)Me]$^+$ ($\mathbf{4}^+$) with AlMe$_3$. Addition of $AlMe_3$ (1 equiv) to a solution of [Ti(N^{t}Bu)(Me$_3$[9]aneN$_3$)Me]$^+$ ($\mathbf{4}^+$) in C_6D_5Br gave quantitative conversion to [Ti(N^{t}Bu)(Me$_3$[9]aneN$_3$)(μ-Me)$_2$AlMe$_2$]$^+$ ($\mathbf{7}^+$). The reaction was conveniently scaled up by treating a CH_2Cl_2 solution of **3** and $AlMe_3$ with [CPh$_3$][BAr$^F_4$] (Scheme 1, Ar^F = C_6F_5) which afforded **7**-BAr$^F_4$ in ca. 50% isolated yield. The NMR spectra were consistent with the C_s symmetrical structure shown in Scheme 1, which has been confirmed by X-ray crystallography. The Ti(μ-Me)$_2$Al bridging methyl groups appear as a singlet (relative integration 6 H) at 0.86 ppm in the ^{1}H spectrum, and the inequivalent terminal Al−Me methyl groups appear at −0.48 ("down" with respect to the Me$_3$[9]aneN$_3$ ligand) and −0.87 ("up") ppm. The corresponding shifts in the ^{13}C NMR spectrum are 23.3, −4.9, and −7.6 ppm, respectively. The average $^1J_{CH}$ values for the bridging and terminal methyl groups are rather similar (110 and 113 Hz in C_6D_5Br; 111 and 113 Hz in CD_2Cl_2). These can be compared to values of 111 Hz for the dimethyl Ti(N^{t}Bu)(Me$_3$[9]aneN$_3$)Me$_2$ (**3**), 116 Hz for the methyl cation $\mathbf{4}^+$, 113 Hz for the adduct [Ti(N^{t}Bu)(Me$_3$[9]aneN$_3$)Me(OPPh$_3$)]$^+$ (all in C_6D_5Br), and 112 and 115 Hz for the bridging and terminal methyl groups of Al_2Me_6 itself.[43] Bochmann has reported $^1J_{CH}$ values of ca. 113−114 Hz (μ-Me) and 114−116 Hz (Al-Me) for the zirconium and hafnium $AlMe_3$ adducts [Cp′$_2$M(μ-Me)$_2$AlMe$_2$]$^+$ (Cp′$_2$ = (η-C$_5$H$_5$)$_2$, Me$_2$Si(indenyl)$_2$, or 1,2-C$_2$H$_4$(indenyl)$_2$; M = Zr or Hf).[12] The IR spectrum of solid **7**-BAr$^F_4$ showed no low-frequency ν(C−H) bands which could have been indicative of significant Ti···H−C agostic interactions.[44,45]

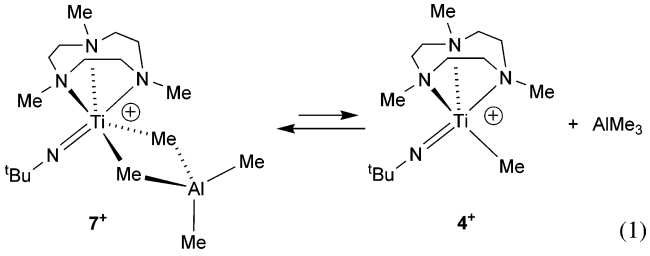

(1)

The ^{1}H and ^{13}C NMR spectra of $\mathbf{7}^+$ were sharp at room temperature, but qualitative 1-dimensional spin saturation transfer (SST) and 2-dimensional EXSY experiments revealed some residual dynamic processes consistent with the dissociative process summarized in eq 1. No exchange was found below 233 K. Norton has recently described a detailed analysis of analogous equilibria in $AlMe_3$ adducts of group 4 metallocenium cations.[20] The room-temperature experiments revealed net site exchange between the cis and trans (with respect to N^{t}Bu) macrocycle NMe groups, the bridging and terminal metal-bound Me groups, and the inequivalent terminal Al−Me groups. When 1 equiv of $AlMe_3$ was added to an NMR sample of $\mathbf{7}^+$, no broadening of the latter's spectrum was observed. The EXSY spectrum, however, showed clear net site exchange between all the metal-bound Me groups of the two organometallic species. These data indicate a dissociatively activated exchange between the free and coordinated $AlMe_3$. Unfortunately, the slow rates of exchange and the inherent instability of $\mathbf{7}^+$ in solution prevented us acquiring data of sufficent quality for a quantitative analysis of the various exchange processes.

Crystals of **7**-BAr$^F_4$ were grown from a CH_2Cl_2 solution, and data were collected at 150 K. This is the first X-ray structure of an $AlMe_3$ adduct of a transition metal alkyl cation. The molecular structure of $\mathbf{7}^+$ is shown in Figure 2, and selected bond distances and angles are given in Table 1. The geometry at Ti(1) and Al(1) is approximately octahedral and tetrahedral, respectively, and the molecular symmetry is approximately C_s in accordance with the solution NMR data. The H atoms of the Ti(μ-Me)$_2$AlMe$_2$ unit were located from Fourier difference maps and positionally and isotropically refined. Within error, the experimental geometries at the two bridging methyl groups C(1) and C(2) are identical with each other and consistent with the DFT-computed structure (**7Q**) discussed below.

The Ti−N distances in $\mathbf{7}^+$ are all shorter than those in the neutral compound Ti(N^{t}Bu)(Me$_3$[9]aneN$_3$)Me$_2$ (**3**)[36] as would

(43) Yamamoto, O. *J. Chem. Phys.* **1975**, *63*, 2988.
(44) Brookhart, M.; Green, M. L. H.; Wong, L.-L. *Prog. Inorg. Chem.* **1988**, *36*, 1.
(45) Scherer, W.; McGrady, G. S. *Angew. Chem., Int. Ed.* **2004**, *43*, 1782.

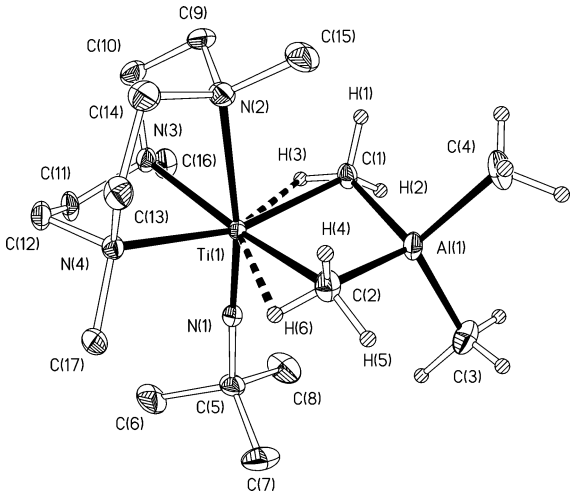

Figure 2. Displacement ellipsoid plot (25% probability) of $[Ti(N^tBu)(Me_3[9]aneN_3)(\mu\text{-}Me)_2AlMe_2]^+$ (**7**$^+$). H atoms other than those of the $AlMe_4$ moiety (shown as spheres of arbitrary radius) are omitted for clarity.

Table 1. Selected Bond Lengths (Å) and Angles (deg) for $[Ti(N^tBu)(Me_3[9]aneN_3)(\mu\text{-}Me)_2AlMe_2]^+$ (**7**$^+$)[42]

Ti(1)−N(1)	1.698(2)	Ti(1)−N(2)	2.413(2)
Ti(1)−N(3)	2.285(2)	Ti(1)−N(4)	2.289(2)
Ti(1)−C(1)	2.344(2)	Ti(1)−C(2)	2.335(2)
Al(1)−C(1)	2.081(2)	Al(1)−C(2)	2.075(2)
Al(1)−C(3)	1.963(3)	Al(1)−C(4)	1.981(3)
Ti(1)···H(3)	2.17(3)	Ti(1)···H(6)	2.17(3)
C(1)−H(1)	0.99(3)	C(1)−H(2)	0.97(3)
C(1)−H(3)	0.97(3)	C(2)−H(4)	0.97(3)
C(2)−H(5)	0.99(3)	C(2)−H(6)	0.98(3)
C(1)−Ti(1)−C(2)	91.24(7)	C(2)−Ti(1)−N(1)	96.26(8)
C(1)−Ti(1)−N(1)	96.61(8)	C(2)−Ti(1)−N(2)	90.34(8)
C(1)−Ti(1)−N(2)	88.90(7)	C(1)−Ti(1)−N(3)	94.69(7)
N(1)−Ti(1)−N(2)	171.29(7)	N(1)−Ti(1)−N(3)	96.91(7)
C(2)−Ti(1)−N(3)	164.83(7)	C(1)−Ti(1)−N(4)	163.85(7)
N(2)−Ti(1)−N(3)	75.84(6)	N(1)−Ti(1)−N(4)	98.52(7)
C(2)−Ti(1)−N(4)	92.71(7)	N(3)−Ti(1)−N(4)	77.92(6)
N(2)−Ti(1)−N(4)	75.43(6)	C(1)−Al(1)−C(3)	112.34(11)
C(1)−Al(1)−C(2)	107.16(8)	C(1)−Al(1)−C(4)	107.66(11)
C(2)−Al(1)−C(3)	112.84(12)	C(3)−Al(1)−C(4)	110.97(12)
C(2)−Al(1)−C(4)	105.47(11)	Ti(1)−C(1)−Al(1)	79.58(7)
Ti(1)−C(2)−Al(1)	79.92(7)		

be expected from the formal positive charge at titanium. The Ti−C distances on the other hand are longer (average 2.339 Å in **7**$^+$ vs 2.213 Å in **3**), which is consistent with the titanium-bound methyls in **7**$^+$ participating in 3-center, 2-electron bonding to aluminum. The terminal Al−Me bonds are shorter (average 1.972 Å) than the bridging ones (average 2.078 Å) for the same reasons, and this is also the case in Al_2Me_6[46,47] and most crystallographically characterized rare earth $AlMe_4$ complexes.[48,49]

The geometry of the two bridging methyl groups is approximately square-based pyramidal with one short Ti···H contact/μ-Me group (each 2.17(3) Å). An analogous geometry was found for the bridging methyl groups in Al_2Me_6 according to a recent neutron diffraction study.[47] In contrast, most AlR_3 adducts of rare earth compounds show (where H atom location has been possible) approximately trigonal bipyramidal geometries for the bridging alkyl groups and two close Ln···H contacts (note in particular the recent neutron diffraction study of $Nd(AlMe_4)_3$[25]). It appears that the modeling of transition metal cations $[L_nM(\mu\text{-}Me)_2AlMe_2]^+$ by neutral, rare earth analogues may only be appropriate to a first approximation in most cases and that the actual orientation of the μ-methyl ligands may differ for transition metal systems. This aspect is discussed in further detail below in the DFT section and Supporting Information.

Reaction of $[Ti(N^tBu)(Me_3[9]aneN_3)Me]^+$ (4$^+$) with $ZnMe_2$. Whereas μ-hydrocarbyl-bridged transition metal adducts of AlR_3 are well-established, there is a paucity of such heterobimetallic species for zinc, even though dialkyl zincs undergo degenerate alkyl group exchange through alkyl-bridged intermediates.[50] The important role of transient zinc alkyl adducts of transition metal alkyl cations in polymerization catalysis was mentioned above in the Introduction. Neutral μ-aryl-bridged Au/Zn bi- and trimetallic compounds have been reported.[51,52] Reaction of $ZnMe_2$ with $RuHCl(PPh_3)_3$ gave an ill-defined Ru−Zn_2−Ru heterotetrametallic species,[53] and that with $IrMe(PMe_3)_4$ gave *fac*-$IrMe_2(ZnMe)(PMe_3)_3$.[54] Bimetallic species involving Ni(μ-Me)Zn interactions have been proposed as intermediates in certain Ni-catalyzed coupling reactions involving organozincs.[55] A fast Zn−Me/W−Me ligand exchange reaction took place between $ZnMe_2$ and the imido tungsten methyl cation $[W(N_2N_{py})(NPh)Me]^+$ (N_2N_{py} = $(2\text{-}NC_5H_4)C(Me)(CH_2NSiMe_3)_2$),[56] as discussed further in the DFT section. The gas-phase reaction between $ZnMe_2$ and $[Cp_2ZrMe]^+$ gave the methylidene-bridged heterobimetallic $[Cp_2Zr(\mu\text{-}CH_2)(\mu\text{-}Me)Zn]^+$ according to ion cyclotron resonance spectrometry.[57] Solution phase attempts to prepare $ZnMe_2$ adducts of $[Cp_2ZrMe]^+$ or $[Cp^*_2ZrMe]^+$ (with $[MeBAr^F_3]^-$ or $[BAr^F_4]^-$ counteranions) were hampered by facile exchange of alkyl and aryl groups between zinc and boron.[34]

Addition of a toluene solution of $ZnMe_2$ (1 equiv) to in situ prepared $[Ti(N^tBu)(Me_3[9]aneN_3)Me]^+$ (**4**$^+$) in C_6D_5Cl gave quantitative conversion to $[Ti(\mu\text{-}N^tBu)(Me_3[9]aneN_3)(\mu\text{-}Me)_2ZnMe]^+$ (**8**$^+$) (Scheme 1). Attempts to isolate this cation were unsuccessful, leading to mixtures of products. Nonetheless, **8**-BAr^F_4 appeared to be moderately stable in solution, and no evidence for exchange of Zn−Me and B−Ar^F groups was observed, in contrast to the isolobal zirconocenium systems.[34] Our inability to isolate **8**-BAr^F_4 is attributed to the inherently weak coordination of $ZnMe_2$ to **4**$^+$. As illustrated in Scheme 1, the lowest energy DFT structure of **8**$^+$ (**8Q** discussed later) featured a N_{imide}···Zn interaction in addition to two Ti(μ-Me)Zn methyl groups, and this is consistent with the following spectroscopic data (see the Supporting Information for various ^{1}H NMR spectra).

(46) Huffman, J. C.; Streib, W. E. *Chem. Commun.* **1971**, 911.
(47) McGrady, G. S.; Turner, J. F. C.; Ibberson, R. M.; Prager, M. *Organometallics* **2000**, *19*, 4398.
(48) Fletcher, D. A.; McMeeking, R. F.; Parkin, D. *J. Chem. Inf. Comput. Sci.* **1996**, *36*, 746 (The United Kingdom Chemical Database Service).
(49) Allen, F. H.; Kennard, O. *Chem. Des. Automat. News* **1993**, *8*, 1, 31.
(50) Nehl, H.; Scheidt, W. R. *J. Organomet. Chem.* **1985**, *289*, 1.
(51) de Graaf, P. W. J.; Boersma, J.; van der Kerk, G. J. M. *J. Organomet. Chem.* **1977**, *127*, 391.
(52) de Graaf, P. W. J.; de Koning, A. J.; Boersma, J.; van der Kerk, G. J. M. *J. Organomet. Chem.* **1977**, *141*, 345.
(53) Cole-Hamilton, D. J.; WIlkinson, G. *J. Chem. Soc., Dalton Trans.* **1977**, 797.
(54) Thorn, D. L.; Harlow, R. L. *J. Am. Chem. Soc.* **1989**, *111*, 2575.
(55) Hratchian, H. P.; Chowdhury, S. K.; Gutierrez-Garcia, V. M.; Amarasinghe, K. K. D.; Heeg, M. J.; Schlegel, H. B.; Montgomery, J. *Organometallics* **2004**, *23*, 4636.
(56) Ward, B. D.; Orde, G.; Clot, E.; Cowley, A. R.; Gade, L. H.; Mountford, P. *Organometallics* **2004**, *23*, 4444.
(57) Siedle, A. R.; Newmark, R. A.; Schroepfer, J. N.; Lyon, P. A. *Organometallics* **1991**, *10*, 400.

The room-temperature ^{1}H NMR spectrum showed that $\mathbf{8}^+$ is highly fluxional at this temperature, in contrast to the situation for $[Ti(N^tBu)(Me_3[9]aneN_3)(\mu\text{-}Me)_2AlMe_2]^+$ ($\mathbf{7}^+$). The macrocycle methyl and methylene groups appeared as very broad signals. A single broad ^{1}H resonance at ca. -0.1 ppm is attributed to the three rapidly exchanging metal-bound methyl groups. The fluxional process presumably involves a rapid dynamic equilibrium between $\mathbf{8}^+$ and separated $\mathbf{4}^+$ and $ZnMe_2$ (eq 2), analogous to that proposed for $\mathbf{7}^+$ (eq 1) and its metallocenium analogues.[20]

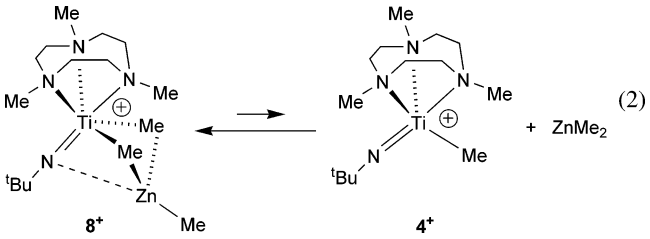

(2)

On cooling of the sample to 233 K, the fluxional process was effectively frozen out, and the expected resonances for a C_s symmetric complex $\mathbf{8}^+$ were observed. The macrocycle NMe groups gave rise to two singlets of integral 6 and 3 H, and the methylene groups were observed as a series of multiplets. At this temperature the metal-bound methyl groups appeared as two singlets at -0.05 ppm (integral 3 H) and -0.14 ppm (integral 6 H), assigned to terminal ZnMe and bridging Ti(μ-Me)$_2$Zn groups, respectively. The shifts of these resonances were noticeably temperature-dependent, and the general broadness of the ^{1}H spectra (including the macrocyclic region) between the low-temperature limit (233 K) and ambient temperature was influenced by sample concentration and/or the presence of any added $ZnMe_2$. It is possible that the position of the dynamic equilibrium shown in eq 2 between $\mathbf{8}^+$ and the separated $\mathbf{4}^+$ and $ZnMe_2$ is influenced by these factors, although at no point was a spectrum showing these separated components obtained.

The ^{13}C shifts for the terminal and bridging methyl groups were -8.2 (^1J = 120 Hz) and 25.7 ppm (^1J = 115 Hz), respectively. The methyl groups of $ZnMe_2$ in the same solvent appear at -0.62 ppm (^1J = 122 Hz) at 233 K. The small 5 Hz reduction in $^1J_{CH}$ for the bridging methyls in $\mathbf{8}^+$ compared to the terminal one is analogous to the situation in $\mathbf{7}^+$, Al_2Me_6, and the metallocenium analogues $[Cp_2M(\mu\text{-}Me)_2AlMe_2]^+$ (2−3 Hz). The relatively high-field ^{13}C shift for the terminal ZnMe group is in the range expected.[58,59]

To our knowledge, this is the first direct observation of a dialkylzinc adduct of a metal alkyl cation. The highly fluxional and labile nature of $\mathbf{8}^+$ at room temperature contrasts with the static structure observed for $\mathbf{7}^+$ and indicates that the coordination of $ZnMe_2$ to $\mathbf{4}^+$ is less thermodynamically favorable than that of $AlMe_3$. As an experimental test of this, a solution of $\mathbf{8}^+$ in C_6D_5Cl was treated with 1 equiv of $AlMe_3$. The $ZnMe_2$ was rapidly and quantitatively displaced from $\mathbf{8}^+$ to form $\mathbf{7}^+$ as illustrated in Scheme 1. These results are consistent with the DFT calculations presented later.

As mentioned, zinc alkyls are important in chain transfer reactions of metal alkyl cations, and so further NMR tube scale reactions of $\mathbf{8}^+$ were carried out. Addition of $ZnMe_2$ (1 equiv) to a C_6D_5Cl solution of $\mathbf{8}^+$ at room temperature gave a single broad, weighted-averaged resonance at ca. -0.3 ppm for the metal-bound methyl groups of $\mathbf{8}^+$ and $ZnMe_2$, consistent with overall exchange between free and coordinated $ZnMe_2$. On cooling of the sample to 253 K, this separated out to those of $\mathbf{8}^+$ (as described above) and free $ZnMe_2$, still slightly broadened. A spin saturation transfer (irradiation at the free $ZnMe_2$ resonance) showed rapid SST into both the terminal *and* bridging methyl sites of the Ti(μ-Me)$_2$ZnMe moiety of $\mathbf{8}^+$ (ratio 1:1.7). Cooling to 233 K (close to the freezing point of C_6D_5Cl) gave further sharpening of the metal-bound methyl resonances. An analogous SST experiment (again irradiating the resonance for free $ZnMe_2$) at this temperature was carried out. Interestingly, this showed exchange predominantly *only* between the terminal Zn−Me group of $\mathbf{8}^+$ and those of free $ZnMe_2$ (ratio 1:0.2 for the terminal and bridging methyls, respectively).

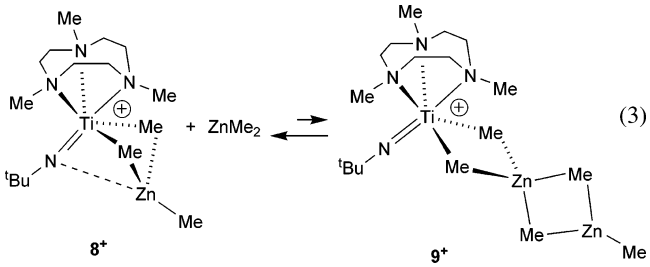

(3)

We were not able to quantify the different independent rates of exchange between the terminal Zn-Me and bridging Ti(μ-Me)Zn groups of $\mathbf{8}^+$ and/or of these with free $ZnMe_2$.[60] Nonetheless, the qualitative SST experiments clearly suggest that *partial* intermolecular alkyl group exchange of dialkylzinc adducts may occur, even in the absence of *complete* exchange of free and coordinated ZnR_2 groups. Equation 3 shows a potentially viable exchange mechanism via an intermediate/transition state $[Ti(N^tBu)(Me_3[9]aneN_3)(\mu\text{-}Me)_2Zn(\mu\text{-}Me)_2ZnMe]^+$ ($\mathbf{9}^+$). In this context we note Bochmann's report that the 3-coordinate zinc methyl cation $[(DAD)ZnMe]^+$ undergoes rapid methyl group exchange with neutral $(DAD)ZnMe_2$, even at -80 °C (DAD = ArNC(Me)C(Me)NAr, Ar = 2,6-$C_6H_3{}^iPr_2$): this is presumed to proceed via a four-coordininate intermediate/transition state of the type $[\{(DAD)ZnMe\}_2(\mu\text{-}Me)]^+$.[58] A number of zinc alkylmetalates containing tetrahedral zinc coordinated to four sp^3-, sp^2-, or sp-hybidized carbons have in fact been crystallographically characterized.[61−64]

Our results may also be relevant to Brintzinger's observation that $ZnMe_2$ has a much greater chain-shortening effect compared to that of $AlMe_3$ when used as a chain transfer agent in certain zirconocene-based copolymerization processes.[33] Thus, in addition to the experimentally proven ability of $AlMe_3$ to bind more tightly to metallocene-like cations than $ZnMe_2$, partial $ZnMe_2$/coordinated ZnR_2 alkyl group exchange is able to occur

(58) Hannant, M. D.; Schormann, M.; Bochmann, M. *J. Chem. Soc., Dalton Trans.* **2002**, 4071.
(59) Looney, A.; Han, R.; Gorrel, I. B.; Cornebise, M.; Yoon, K.; Parkin, G. *Organometallics* **1995**, *14*, 274.
(60) For example, even at 233 K it is clear that bridge Ti−Me−Zn/terminal Zn−Me exchange (likely via eq 2) competes with terminal Zn−Me/free ZnMe2 exchange (eq 3).
(61) Edwards, A. J.; Fallaize, A.; Raithby, P. R.; Rennie, M.-R.; Steiner, A.; Verhorevoort, K. L.; Wright, D. S. *J. Chem. Soc., Dalton Trans.* **1996**, 133.
(62) Fröhlich, H.-O.; Kosan, B.; Miller, B.; Hiler, W. *J. Organomet. Chem.* **1992**, *441*, 177.
(63) Cremer, U.; Pantenburg, I.; Ruschewitz, U. *Inorg. Chem.* **2003**, *42*, 7716.
(64) Rijnberg, E.; Jastrzebski, J. T. B. H.; Boersma, J.; Kooijman, H.; Veldman, N.; Spek, A. L.; van Koten, G. *Organometallics* **1997**, *16*, 2239.

without cleavage of either metal−μ-alkyl bond. In contrast, $AlMe_3$ appears to only exchange with coordinated AlR_3 via a dissociative mechanism.

Reaction of [Ti(N^{t}Bu)(Me$_3$[9]aneN$_3$)Me]$^+$ (4$^+$) with Cp$_2$ZrMe$_2$. Bochmann has reported that the cation $[Cp_2ZrMe]^+$ reacts with Cp_2ZrMe_2 to form the homobimetallic methyl-bridged species $[Cp_2ZrMe(\mu\text{-}Me)ZrMeCp_2]^+$.[12] As mentioned, **4**$^+$ forms an analogous homobimetallic derivative **6**$^+$ (Figure 1) on reaction with Ti(N^{t}Bu)(Me$_3$[9]aneN$_3$)Me$_2$ (**3**).[39] The reaction of **4**$^+$ with Cp_2ZrMe_2 was therefore carried out with the expectation of forming a heterobimetallic cation of the type $[Ti(N^tBu)(Me_3[9]aneN_3)Me(\mu\text{-}Me)ZrMeCp_2]^+$. Surprisingly, and in contrast to the reactions with $AlMe_3$ and $ZnMe_2$, when in situ generated **4**$^+$ was treated with Cp_2ZrMe_2, the new heterobimetallic complex $[Ti(N^tBu)\{Me_2(\mu\text{-}CH_2)[9]aneN_3\}(\mu\text{-}CH_2)ZrCp_2][B(C_6F_5)_4]$ (**10**-BAr^F$_4$) (Scheme 1) was obtained in 74% yield. We were not able to obtain diffraction-quality crystals of **10**-BAr^F$_4$, and the structure is assigned on the basis of spectroscopic and analytical data and is evidently the product of a net double C−H bond activation.

The NMR data for the cation **10**$^+$ showed that it has a C_1 symmetric structure. The ^{1}H NMR spectrum featured resonances for two inequivalent Cp rings, and the two remaining (i.e. nonmetalated) macrocycle NMe groups are also inequivalent. The N(μ-CH$_2$)Zr bridging methylene group was observed as a pair of mutually coupled doublets at 3.05 and 2.28 ppm, while the methylene bridging between the two metal centers appeared as a pair of mutually coupled doublets at somewhat lower field (δ = 6.80 and 5.82 ppm). The corresponding ^{13}C resonance (assigned by a ^{1}H−^{13}C correlation spectrum) also had a rather low field chemical shift (202.2 ppm). These values for the Ti(μ-CH$_2$)Zr group in **10**$^+$ can be compared favorably to bridging methylene resonance shifts of 7.63 (^{1}H) and 205.7 (^{13}C) ppm in the heterobimetallic complex $Cp_2Ti(\mu\text{-}CH_2)_2ZrCp_2$[65] and of 7.13 (average ^{1}H) and 188.19 (^{13}C) ppm in the cationic bimetallic species $[Cp_2(\mu\text{-}\eta^5,\eta^5\text{-}C_{10}H_8)Zr_2(\mu\text{-}Me)(\mu\text{-}CH_2)]^+$.[66]

In principle, the Ti(μ-CH$_2$)Zr methylene moiety in **10**$^+$ could arise from either a Ti−Me or a Zr−Me group. To clarify the situation, the reaction between in situ generated **4**$^+$ and $Cp_2Zr(CD_3)_2$ was followed on the NMR tube scale in C_6D_5Br. The product spectrum was indistinguishable from that obtained with natural abundance Cp_2ZrMe_2, and in particular, the Ti(μ-CH$_2$)Zr methylene resonances at 6.80 and 5.82 ppm were of the correct intensity relative to the rest of the spectrum. The ^{2}H NMR spectrum of the product (after evaporation of the volatiles and redissolving in CH_2Cl_2) showed no accumulation of deuterium in the Ti(μ-CH$_2$)Zr (or any other) site. Therefore, it is apparent that both methyl groups of Cp_2ZrMe_2 (or $Cp_2Zr(CD_3)_2$) are lost in the formation of **10**$^+$, although the mechanistic details of this reaction are not clear.

The intermolecular double C−H bond cleavage reaction leading to *hetero*bimetallic **10**$^+$ is very unusual. *Homo*bimetallic methylene-bridged cations have been prepared from cationic alkyl precursors or intermediates: reaction of $Cp_2(\mu\text{-}\eta^5,\eta^5\text{-}C_{10}H_8)Zr_2Me_4$ with $[CPh_3][BAr^F{}_4]$ at 213 K formed $[Cp_2(\mu\text{-}\eta^5,\eta^5\text{-}C_{10}H_8)Zr_2(\mu\text{-}Me)(\mu\text{-}CH_2)]^+$;[66] warming a solution of $[Cp^*Zr\{MeC(N^tBu)(NEt)\}Me]^+$ to room temperature in the presence of $PhNMe_2$ afforded $[Cp^*{}_2Zr_2\{MeC(N^tBu)(NEt)\}_2(\mu\text{-}Me)(\mu\text{-}CH_2)]^+$;[67] allowing a solution of $[Cp^R{}_2Ti_2(NC^tBu_2)_2Me_2(\mu\text{-}Me)]^+$ (Cp^R = Cp, Cp*, or $C_5Me_4SiMe_3$) to stand at room temperature for several hours afforded $[Cp^R{}_2Ti_2(NC^tBu_2)_2(\mu\text{-}Me)(\mu\text{-}CH_2)]^+$ and methane.[68] We note also that concomitant C−H bond activation of a triazacyclononane NMe group and metal−alkyl bond cleavage has recently been observed for a neutral dilanthanum complex formed by reaction of in situ generated $La(CH_2SiMe_3)_3(THF)_n$ and ^{t}BuN(H)SiMe$_2$(Me)$_2$[9]aneN$_3$.[69]

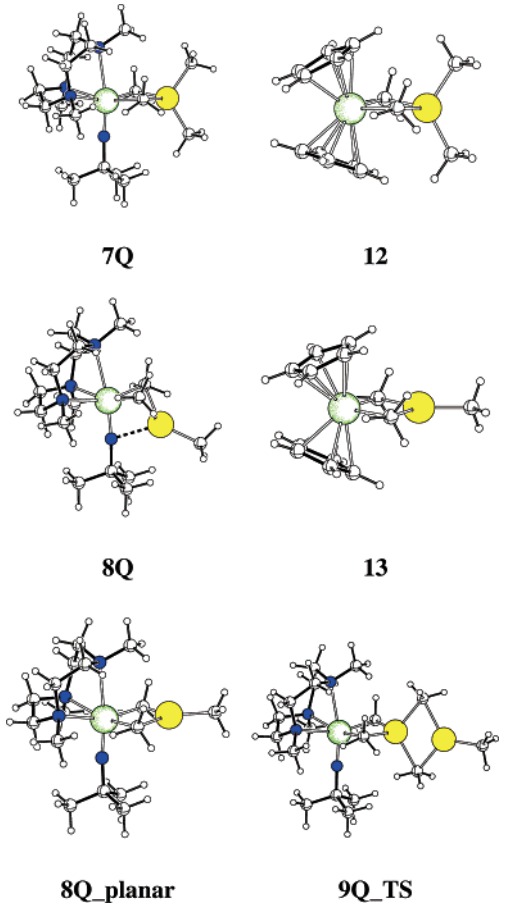

Figure 3. B3PW91-optimized geometry for $[Ti(N^tBu)(Me_3[9]aneN_3)(\mu\text{-}Me)_2AlMe_2]^+$ (**7Q**), $[Ti(N^tBu)(Me_3[9]aneN_3)(\mu\text{-}Me)_2ZnMe]^+$ (**8Q** and **8Q_planar**), $[Cp_2Ti(\mu\text{-}Me)_2AlMe_2]^+$ (**12**), $[Cp_2Ti(\mu\text{-}Me)_2ZnMe]^+$ (**13**), and $[Ti(N^tBu)(Me_3[9]aneN_3)(\mu\text{-}Me)_2Zn(\mu\text{-}Me)_2ZnMe]^+$ (**9Q_TS**).

DFT Studies of Heterobimetallic Methyl-Bridged Cations.[70] Calculated Geometries of the AlMe$_3$ and ZnMe$_2$ Adducts 7$^+$ and 8$^+$. The methyl-bridged heterobimetallic cation **7**$^+$ has been characterized by X-ray crystallography, and its structure serves as a test for the computational methodology used in this work. The full system $[Ti(N^tBu)(Me_3[9]aneN_3)(\mu\text{-}Me)_2AlMe^2]^+$ was optimized at the B3PW91 level as model complex **7Q** (Figure 3); selected geometric parameters are listed in Table 2. Further details for **7Q** and all the computed structures are given in the Supporting Information. The overall agreement

(65) van de Heisteeg, B. J. J.; Schat, G.; Akkerman, O. S.; Bickelhaupt, F. *Organometallics* **1985**, *4*, 1141.
(66) Bochmann, M.; Cuenca, T.; Hardy, D. T. *J. Organomet. Chem.* **1994**, *484*, C10.
(67) Keaton, R. J.; Jayaratne, K. C.; Fettinger, J. C.; Sita, L. R. *J. Am. Chem. Soc.* **2000**, *122*, 12909.
(68) Zhang, S.; Piers, W. E. *Organometallics* **2001**, *20*, 2088.
(69) Tazelaar, C. G. J.; Bambirra, S.; van Leusen, D.; Meetsma, A.; Hessen, B.; Teuben, J. H. *Organometallics* **2004**, *23*, 936.
(70) In the DFT computed structures, labels "Q" indicate that the methyl groups of the triazacyclononane and the *tert*-butyl group of the imide were included in the calculation. Labels "q" indicate that these were not included and instead substituted by H and Me, respectively.

Table 2. Selected Geometrical Parameters (Distances in Å) for [Ti(N^{t}Bu)(Me$_3$[9]aneN$_3$)(μ-Me)$_2$AlMe$_2$]$^+$ (**7Q**), [Cp$_2$Ti(μ-Me)$_2$AlMe$_2$]$^+$ (**12**), [Ti(N^{t}Bu)(Me$_3$[9]aneN$_3$)(μ-Me)$_2$ZnMe]$^+$ (**8Q** and **8Q_planar**), [Cp$_2$Ti(μ-Me)$_2$ZnMe]$^+$ (**13**), [Ti(NMe)(H$_3$[9]aneN$_3$)(μ-Me)$_2$AlMe$_2$]$^+$ (**7q**), [Ti(μ-NMe)(H$_3$[9]aneN$_3$)Me(μ-Me)ZnMe]$^+$ (**8q**), [Ti(μ-N^{t}Bu)(Me$_3$[9]aneN$_3$)Me(μ-Me)AlMe$_2$]$^+$ (**7Q′**), and [Ti(μ-NMe)(H$_3$[9]aneN$_3$)Me(μ-Me)AlMe$_2$]$^+$ (**7q′**)[a]

parameters	7Q	12	8Q	8Q_planar	13	7q	8q	7q′	7Q′
Ti−X(1)	2.290	2.270	2.202	2.296	2.270	2.280	2.164	2.111	2.107
Ti−X(2)	2.289	2.270	2.223	2.296	2.269	2.281	2.211	2.256	2.234
closest Ti···H for C(1)	2.21	2.29	b	2.171	2.29	2.24	b	b	b
closest Ti···H for C(2)	2.20	2.29	2.390	2.173	2.26	2.21	2.51	2.37, 2.81	2.49, 2.64
Ti−N(1)	1.676		1.718	1.678		1.676	1.734	1.752	1.764
N(1)···X	3.437		2.296	3.396		3.397	2.130	2.012	2.047
C(1)−X	2.119	2.157	2.356	2.115	2.152	2.130	2.727	3.967	3.635
C(2)−X	2.127	2.157	2.246	2.117	2.145	2.134	2.302	2.190	2.178
X−C$_{terminal}$	1.985, 1.973	1.963, 1.966	1.949	1.949	1.938	1.978, 1.968	1.938	1.964, 1.977	1.976, 1.979

[a] The numbering scheme for the bridging carbons is based on that used in the experimental structure of **7**$^+$ (Figure 2). [b] None less than 2.60 Å.

between experimental (**7**$^+$) and calculated values (**7Q**) is excellent (see Tables 1 and 2), and such an accuracy is expected to hold for the systems to be described later where no X-ray structures are available.

Experimentally, the reaction between [Ti(N^{t}Bu)(Me$_3$[9]aneN$_3$)Me]$^+$ (**4**$^+$) and ZnMe$_2$ gave the heterobimetallic adduct **8**$^+$ (Scheme 1), which contains a Ti(μ-Me)$_2$ZnMe unit on the basis of low-temperature ^{1}H and ^{13}C NMR data. The DFT-computed geometry for the corresponding model (**8Q**) is shown in Figure 3, and selected geometrical parameters are given in Table 2. The structure of **8Q** is fully consistent with all the available NMR data for **8**$^+$. At first sight, the geometry for **8Q** is analogous to that of **7Q** with two methyl groups bridging the Ti(N^{t}Bu)(Me$_3$[9]aneN$_3$) and ZnMe fragments. However, the Ti−C distances for the bridging methyls are somewhat inequivalent (2.202, 2.223 Å) and, on average, substantially shorter than those in **7Q** (2.290, 2.289 Å). There is a much larger asymmetry in the Zn−μ-C bond distances (2.356 and 2.246 Å) where the longest Zn−C bond corresponds to the methyl group having the shortest Ti−C bond (atom C(1) in Table 2). Unsurprisingly, the two bridging Zn−Me distances are considerably longer than the terminal Zn−Me distance (1.949 Å). Despite the steric bulk of the *tert*-butyl substituent in **8Q**, the Ti(μ-C)$_2$Zn moiety is highly nonplanar (fold angle 103.3°) and there is a significantly short Zn···N bonding contact with the imido nitrogen (2.297 Å), which contrasts with the long, nonbonded Al···N(1) distance in **7Q** (3.437 Å). Therefore, the ZnMe$_2$ adduct **8**$^+$ is better formally described as a [Ti(μ-N^{t}Bu)(Me$_3$[9]aneN$_3$)(μ-Me)$_2$ZnMe]$^+$ complex with simultaneous bridging methyls and a Zn···N$_{imide}$ interaction. Although one of the bridging methyl groups (C(1), Table 2) is further away from Zn, it is still well within bonding distance rendering mutual exchange of the two methyl groups facile as indicated by the experimental observation of equivalent Ti(μ-Me)$_2$Zn methyl groups at room temperature. The coordination geometries of the bridging methyl groups in **7Q** and **8Q** are discussed further in the Supporting Information.

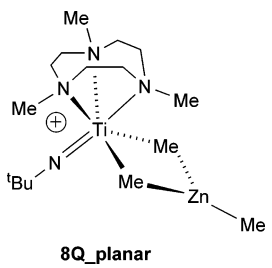

8Q_planar

Forcing the Ti(μ-C)$_2$Zn core to be planar yielded a related structure, **8Q_planar**, lying only 8 kJ mol^{-1} above **8Q** (Figure 3). The geometric parameters of **8Q_planar** (Table 2) are very similar to those of **7Q** with regards to the bridging methyls, and the N$_{imide}$···Zn distance is 1.1 Å longer than that in **8Q**.

The transition state (**9Q_TS**) for exchange of the terminal Zn−Me group of **8Q** with ZnMe$_2$ has been located on the potential energy surface, and its geometry is shown in Figure 3. The transition state vector is a metathesis-like motion, and the geometry of the Zn(μ-Me)$_2$Zn is that of a lozenge with alternating long (2.242 and 2.202 Å) and short (2.172 and 2.169 Å) Zn−C bond distances. The energy of **9Q_TS** with respect to separated **8Q** and ZnMe$_2$ is 53.4 kJ mol^{-1}, in agreement with an exchange observable by NMR at low temperature. Moreover, the energy for complete dissociation of ZnMe$_2$ from **8Q** amounts to 41.3 kJ mol^{-1}; thus, both dissociative exchange of coordinated and free ZnMe$_2$ and associative exchange of just the terminal Zn−Me group through **9Q_TS** possess similar activation parameters. Therefore, the alkyl group exchange processes observed experimentally are a combination of two distinct events (eqs 2 and 3), and the relative contribution of each component is influenced differently by the temperature and the concentration of free ZnMe$_2$ as one process is dissociative and the other associative.

The formation of **8Q** can be explained easily since the HOMO and HOMO-1 of the monomethyl cation **4**$^+$ are the Ti−N$_{imide}$ π orbitals centered on the imido N atom. Consequently, this confers to **4**$^+$ some Lewis base character that can be used to interact with Lewis acids such as ZnMe$_2$ (or AlMe$_3$ as discussed later), provided that the steric repulsion by the imido N-substituent is not prohibitive.

To evaluate the influence of the steric bulk at Ti, we have considered the smaller model complexes [Ti(NMe)(H$_3$[9]aneN$_3$)(μ-Me)$_2$AlMe$_2$]$^+$ (**7q**) and [Ti(μ-NMe)(H$_3$[9]aneN$_3$)Me(μ-Me)ZnMe]$^+$ (**8q**). These have H atoms in place of the *tert*-butyl and macrocycle methyl groups, and so many steric repulsions are alleviated. For **7q**, the structure is not significantly different from that of the more sterically encumbered model **7Q**. For **8q**, however, the Zn···N interaction develops further (2.130 Å) and the already lengthened μ-Me···Zn bond of **8Q** (2.356 Å) elongates to 2.727 Å with a concomitant shortening of Ti−Me (2.164 Å). In addition, the Ti═N$_{imide}$ distance in **8q** (1.734 Å) is significantly longer than in **8Q** (1.718 Å) or **7q** (1.676 Å) as a consequence of the strong N$_{imide}$ interaction with the Zn. The DFT structure for **8q** is analogous to that calculated by DFT for the phenylimido species [W(μ-NPh)(N$_2$N$_{py}$)Me(μ-

Me)ZnMe]$^+$ (**11**$^+$),[56] proposed as a transient intermediate in the facile W−Me/Zn−Me group exchange reaction between the methyl cation [W(NPh)(N_2N_{py})Me]$^+$ and $ZnMe_2$.

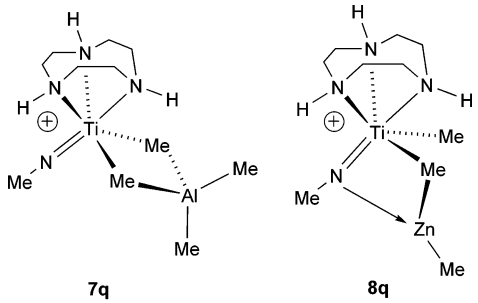

7q **8q**

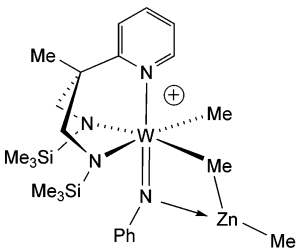

11$^+$

Comparisons with the Titanocenium Analogues [Cp_2Ti(μ-Me)$_2$AlMe$_2$]$^+$ (12) and [Cp_2Ti(μ-Me)$_2$ZnMe]$^+$ (13). We showed previously that the fragment [Ti(N^{t}Bu)(Me$_3$[9]aneN$_3$)]$^{2+}$ is isolobal with [Cp_2Ti]$^{2+}$.[39] We have also given an account of the synthesis and electronic structure of the 14 valence electron methyl cation [Ti(N^{t}Bu)(Me$_3$[9]aneN$_3$)Me]$^+$ (**4**$^+$), together with a comparison with the isoelectronic titanocenium species [Cp_2TiMe]$^+$. Despite the general isolobality of the fragments, the titanium center in [Cp_2Ti]$^{2+}$ has a much larger effective electronegativity than that in [Ti(N^{t}Bu)(Me$_3$[9]aneN$_3$)]$^{2+}$, and there are subtle but significant differences in the shapes and relative energies of their three lowest unoccupied orbitals. These had important consequences for the geometrical, α-agostic bonding, and NMR properties of the corresponding monoalkyl cations. Therefore, given the importance of group 4 metallocenium cations [Cp_2M(μ-Me)$_2$AlMe$_2$]$^+$ in general, and the growing interest in the role of dialkylzinc compounds in cationic Ziegler−Natta olefin polymerization systems, we also studied computationally $AlMe_3$ and $ZnMe_2$ adducts of [Cp_2TiMe]$^+$.

The real $AlMe_3$ adduct [Cp_2Ti(μ-Me)$_2$AlMe$_2$]$^+$ (modeled as **12**) has been described previously,[17,20] but no structural data were obtained. The dimethylzinc adduct [Cp_2Ti(μ-Me)$_2$ZnMe]$^+$ (**13**) has not been reported experimentally. As mentioned, attempts to prepare zirconium analogues of **13** were hampered by anion degradation reactions.[34] Although a DFT-computed geometry for [Cp_2Zr(μ-Me)$_2$AlMe$_2$]$^+$ has been briefly mentioned,[16] no bonding or other analyses were described. The complexes [Cp_2Ti(μ-Me)$_2$XMe$_n$]$^+$ (X = Al, n = 2, **12**; X = Zn, n = 1, **13**) were optimized using DFT. Their structures are shown in Figure 3 and selected geometric parameters are given in Table 2, where they are compared with those for **7Q** and **8Q**.

As expected from their isolobal relationship, the basic geometry of [Cp_2Ti(μ-Me)$_2$AlMe$_2$]$^+$ (**12**) is rather similar to that of [Ti(N^{t}Bu)(Me$_3$[9]aneN$_3$)(μ-Me)$_2$AlMe$_2$]$^+$ (**7**$^+$, **7Q**). The Ti(μ-Me)$_2$Al moiety of **12** is nonplanar, having a fold angle of 166.0° (cf. 163.0° in **7**$^+$ and 165.5° in **7Q**). Furthermore, this

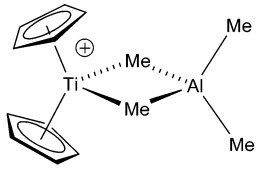

12

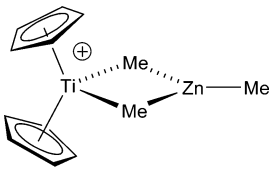

13

puckering persists in the smaller model complex [Ti(NMe)(H$_3$[9]aneN$_3$)(μ-Me)$_2$AlMe$_2$]$^+$ (**7q**), which is sterically less encumbered than **7Q** (Ti(μ-C)$_2$Al fold angle = 164.0°). Interestingly, such puckered metallacyclic cores have been observed to different extents in rare earth metallocenes, Cp$^R{}_2$M(μ-Me)$_2$AlMe$_2$ (Cp^R = Cp or substituted cyclopentadienyl; M = Yb (fold angle 163.4°), Y (162.9°), Sc (two examples, 161.9 and 174.3°)).[23,71,72] In other $AlMe_3$ adducts the M(μ-Me)$_2$AlMe$_2$ is planar (e.g. Nd(AlMe$_4$)$_3$,[25] (ArO)$_2$Lu(μ-Me)$_2$AlMe$_2$ (Ar = 2,6-C$_6$H$_3$^{t}Bu$_2$)[31]), as is also the case for Al_2Me_6 itself.[46,47]

The Ti−C and Al−C bond distances for the bridging methyls differ between **7Q** and **12**. Cation **12** exhibits shorter Ti−C (2.270 Å) and longer Al−C (2.157 Å) bond distances than **7Q** (ca. 2.290 and 2.123 Å, respectively). Similar trends in Ti−Me distances are found in the X-ray structures of the neutral dimethyls Ti(N^{t}Bu)(Me$_3$[9]aneN$_3$)Me$_2$ (**3**, average 2.213 Å)[42] and Cp_2TiMe_2 (average 2.175 Å)[73] and also in the DFT structures of [Ti(N^{t}Bu)(Me$_3$[9]aneN$_3$)Me]$^+$ (2.109 Å) and [Cp_2TiMe]$^+$ (2.069 Å).[39]

The DFT geometry of the $ZnMe_2$ adduct [Cp_2Ti(μ-Me)$_2$ZnMe]$^+$ (**13**) is analogous to that of **12**. The Ti−Me distances are identical with those in **12**. Notably, the Ti(μ-C)$_2$Zn unit of **13** is effectively planar, having a fold angle of 178.8° (cf. 163.0−166.0° in **7**$^+$, **7Q**, **7q**, and **12**). This contrasts strongly with the position for [Ti(μ-N^{t}Bu)(Me$_3$[9]aneN$_3$)(μ-Me)$_2$ZnMe]$^+$ (**8Q**, fold angle 103.3°) and emphasizes the apparent importance of the N_{imide}···Zn interaction in this system.

Electronic Structures of the Adducts. As mentioned, the DFT structure of [Cp_2Zr(μ-Me)$_2$AlMe$_2$]$^+$ has been described,[16] but little detail was provided. We also note computational studies of Al_2Me_6[74] and the "polyagostic"[24] aluminate Y(AlMe$_4$)$_3$.[26] For this latter system the authors advanced computational evidence for significant covalency/delocalization in the Y−μ-C−Al bonds and hypervalent character for the bridging carbons. Notably, the electron density at the Y−μ-C bond critical point (CP) was only slightly less than that at the Al−μ-C bond CP. However, while the bridging methyls have two C−H bonds oriented toward Y with short Y···H contacts (average 2.42 Å), no Y···H

(71) Day, M. W.; Bercaw, J. E; Zubris, D. L. Private communication to the Cambridge Structural Database, deposition no. CCDC 103059: Cambridge Crystallographic Data Centre, 12 Union Road, Cambridge, U.K.
(72) Day, M. W.; Schofer, S. J.; Bercaw, J. E. Private communication to the Cambridge Structural Database, deposition no. CCDC 192902: Cambridge Crystallographic Data Centre, 12 Union Road, Cambridge, U.K.
(73) Thewalt, U.; Wohrle, T. *J. Organomet. Chem.* **1994**, *464*, C17.
(74) Berthomieu, D.; Bacquet, Y.; Pedocchi, L.; Goursot, A. *J. Phys. Chem. A* **1998**, *102*, 7821.

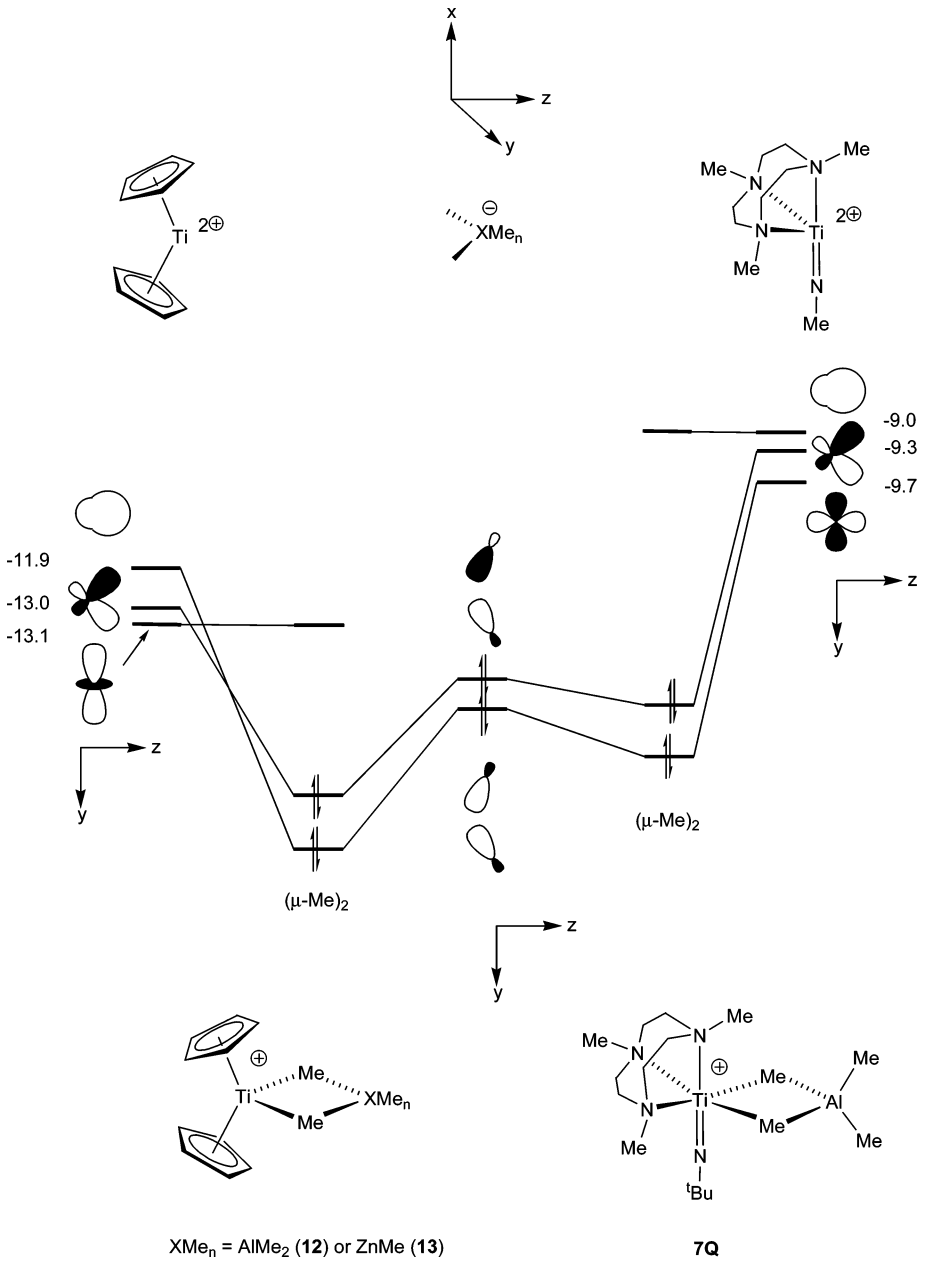

Figure 4. Schematic fragment MO interaction diagram for the Ti(μ-Me)$_2$XMe$_n$ subunit constructed from $[Cp_2Ti^2]^+$ (left) or $[Ti(N^tBu)(Me_3[9]aneN_3)]^{2+}$ and $[Me_2XMe_n]^-$ (X = Al, n = 2; X = Zn, n = 1). MO energies (eV) are obtained from DFT calculations on the respective fragments.[39] Note that the orbitals are viewed in projection onto the *yz* plane for clarity.

bond CP was found and the difference between the C−H bond distances was insignificant (Δ_{C-H} less than 0.01 Å). See the Supporting Information for a detailed discussion of the Ti···H interactions in the complexes studied herein and of bridging methyl group geometries in general for $AlMe_3$ adducts of metal complexes.

Figure 4 shows a schematic MO diagram for the interaction of a $[Cp_2Ti]^{2+}$ or $[Ti(N^tBu)(Me_3[9]aneN_3)]^{2+}$ fragment with a distorted $AlMe_4^-$ or $ZnMe_3^-$ moiety, forming $[Cp_2Ti(\mu\text{-}Me)_2XMe_n]^+$ (XMe_n = $AlMe_2$ (**12**) or ZnMe (**13**)) or $[Ti(N^tBu)(Me_3[9]aneN_3)(\mu\text{-}Me)_2AlMe_2]^+$ (**7Q**), respectively. We reported previously that the lowest unoccupied MOs of $[Cp_2Ti]^{2+}$ lie at significantly lower energy than those of $[Ti(N^tBu)(Me_3[9]aneN_3)]^{2+}$ as illustrated in Figure 4.[39] The highest occupied MOs of $AlMe_4^-$ or $ZnMe_3^-$, distorted with two elongated metal−carbon bonds, are the in-phase and out-of-phase linear combination of two essentially C-centered lone pairs. Because of the specific shapes and energies of the frontier orbitals of the two different titanium fragments, the main Ti−μ-Me interactions differ. For $[Cp_2Ti(\mu\text{-}Me)_2XMe_n]^+$ (**12**, **13**), these involve the LUMO+1 and LUMO+2 of $[Cp_2Ti]^{2+}$ (as is typical for Cp_2MX_2 type compounds[75]). In contrast, for $[Ti(N^tBu)(Me_3[9]aneN_3)(\mu\text{-}Me)_2AlMe_2]^+$ the LUMO and LUMO+1 of $[Ti(N^tBu)(Me_3[9]aneN_3)]^{2+}$ are better spatially and energetically disposed for Ti−μ-Me interactions. Due to the lower energy of the frontier MOs of $[Cp_2Ti]^{2+}$, the interaction with $AlMe_4^-$ leads to a more covalent character for the Ti−C bond and shorter Ti−C bond distances. This is again an illustration of the more electrophilic nature of $[Cp_2Ti]^{2+}$. The qualitative MO diagram also helps to explain the differences observed for the orientation

(75) Lauher, J. W.; Hoffmann, R. *J. Am. Chem. Soc.* **1976**, *98*, 1729.

Table 3. Selected Atomic Contributions (%) of the Main Contributors to the Natural Localized Molecular Orbitals (NLMOs) and Hybridization (Hyb) at C for the Ti−C Bonds in $[Ti(N^tBu)(Me_3[9]aneN_3)(\mu\text{-}Me)_2AlMe_2]^+$ (**7Q**), $[Cp_2Ti(\mu\text{-}Me)_2AlMe_2]^+$ (**12**), $[Ti(N^tBu)(Me_3[9]aneN_3)(\mu\text{-}Me)_2ZnMe]^+$ (**8Q**), and $[Cp_2Ti(\mu\text{-}Me)_2ZnMe]^+$ (**13**) (X = Al (**7Q**, **12**) or Zn (**8Q**, **13**))[a]

compd	bridging carbon	% Ti	% C	% X	hyb C
Al_2Me_6			78.4	10.0, 10.5	$sp^{2.4}$
			78.4	10.0, 10.5	$sp^{2.4}$
7Q	C(1)	10.8	78.2	10.3	$sp^{2.4}$
	C(2)	10.8	78.9	8.9	$sp^{2.4}$
12	C(1)	21.0	70.8	6.7	$sp^{2.77}$
	C(2)	20.9	70.8	6.8	$sp^{2.77}$
8Q	C(1)	17.2	79.3	2.2	$sp^{2.44}$
	C(2)	16.0	79.0	3.4	$sp^{2.59}$
13	C(1)	24.6	70.2	3.2	$sp^{3.1}$
	C(2)	23.9	70.4	3.6	$sp^{3.1}$

[a] For comparison NLMO contributors to the Al−C bonds in Al_2Me_6 are also given.The labels for C(1) and C(2) are as for Table 2.

of the Ti···H−C interactions in **12** and **13** vs **7Q** or **7q** and, hence, the geometries at the bridging carbon (see the Supporting Information for further details).

The Al−μ-Me−Al bonding in Al_2Me_6 is considered to be of the classical 3 center−2 electron (3c−2c) type.[74] As mentioned, the Y−μ-Me−Al bonding has also been analyzed[26] and revealed a 3c−2c bond, polarized toward Al as the more electronegative metal. We have analyzed the Ti−μ-Me−X bonding in **7Q**, **12**, **8Q**, and **13** using NBO procedures. These found either 3c−2e Ti−μ-Me−X bonds (**7Q**) or Ti−C bonds strongly polarized toward the bridging carbon (**12**, **8Q**, or **13**). However, in the latter cases, several strong 2nd order perturbation terms associated with donation from σ(Ti−C) to Al- or Zn-centered orbitals were present, leading to hyperconjugative contributions that are clearly visible in the composition of the natural localized molecular orbitals (NLMOs). Table 3 presents the composition of the NLMOs associated with the Ti−C bonds of the bridging methyls, together with the hybridization of the C atom in the respective NLMOs. An equivalent analysis for Al_2Me_6 using the same methodology is also given for comparison.

The NLMO atomic contributions indicate that the Ti−μ-C−Al interaction in **12** is more localized than in **7Q**, with considerably less participation by the Al atom. The bonding situation is rather more delocalized in **7Q** with approximately equal atomic contributions from Ti and Al. For **7Q** (as for Al_2Me_6 iteself), the M−μ-Me−M′ interaction can accurately be described as a 3c−2e bond. These results indicate that, in **7Q**, Ti and Al are of similar electronegativity, whereas Ti is more electronegative than Al in the metallocene system **12**. This is in accord with our previous analysis of compounds containing the Cp_2Ti and $Ti(N^tBu)(Me_3[9]aneN_3)$ fragments and may also be anticipated from the MO diagram in Figure 4. Interestingly, the hybridization of the bridging carbon in **7Q** is the same as in Al_2Me_6 but somewhat different from that in **12**. The reduced 2s AO contribution in the Ti−C bond of **12** is also consistent with the greater electronegativity of the metal center in this case.

For the $ZnMe_2$ adducts **8Q** and **13**, Zn contributions to the bridging methyl bonding are much weaker than for the $AlMe_3$ adducts, and the Ti−C bonds are more heavily polarized toward Ti, albeit still essentially developed on C (Table 3). There is thus increased covalent character between Ti and C for the $ZnMe_2$ adducts as illustrated by the values of atomic contributions (Table 3). Indeed, the $ZnMe_2$ adducts could almost be described as the result of the interaction between a neutral dimethyl complex and the $ZnMe^+$ moiety. The Zn atom participates in the bonding mainly through its valence s orbital, and thus, there is no preferred geometry of interaction. When a secondary interaction, such as donation from one Ti−N π-bond of the imido to Zn, is possible, the necessary geometry reorganization to accommodate the new interaction is easy. In fact, the Ti−N_{imide} NLMO describing one of the π-bonds of the Ti═NR linkage does indeed contain 2.1% Zn character as a result of the N_{imide}···ZnMe interaction.

Thermodynamic Aspects of Adduct Formation. It is of interest to evaluate the relative energies of adduct formation between $AlMe_3$ and $ZnMe_2$ and the various titanium methyl cations, $[Cp_2TiMe]^+$, $[Ti(N^tBu)(Me_3[9]aneN_3)Me]^+$, and $[Ti(NMe)(H_3[9]aneN_3)Me]^+$, which we have studied experimentally or/and by DFT previously.[39] The formation energies (ΔE) are listed in Table 4 and range from −41.3 to −98.4 kJ mol^{-1} for the adducts so far discussed. The dissociation energy (by DFT) of Al_2Me_6 is computed to be 66 kJ mol^{-1}, and so in general the formation of all of the products listed is likely to be enthalpically favored.

As anticipated from the preceding analysis of the electronic structures, formation of the $AlMe_3$ adducts is thermodynamically more favored than formation of the $ZnMe_2$ adducts. This is also in agreement with the experimental isolation of **7**-$BAr^F{}_4$ (but only NMR observation of the labile **8**-$BAr^F{}_4$) and the facile displacement of $ZnMe_2$ from $\mathbf{8}^+$ by $AlMe_3$ (Scheme 1). Formation of **12** is thermodynamically more exothermic than formation of its isolobal analogue **7Q**, and formation of **13** is more exothermic than formation of **8Q**. However, when the sterically less encumbered models **7q** and **8q** are considered, it can been seen that formation of the imido-supported systems is more favored than the corresponding metallocene analogues. The difference between the formation energies of **7Q** and **8Q** (29.1 kJ mol^{-1}) is very close to that between **12** and **13** (31.2 kJ mol^{-1}), despite the rather different geometry of **8Q**.

To shed more light on the energetics of the adduct formation process, the thermodynamic cycle shown in Figure 5 was considered and the relevant energies are listed in Table 4. Formation of the adducts formally requires the following: (i) deformation of the cationic titanium monomethyl complex to open a coordination site (ΔE_{def}(Ti)); (ii) deformation of XMe_n (X = Al, n = 3; X = Zn, n = 2) to accommodate the bridging geometry (ΔE_{def}(X)); (iii) interaction between the two fragments in the geometry they adopt in the complex (ΔE_{int}(Ti···X)).

We consider first the $AlMe_3$ adducts **7Q**, **7q**, and **12**. For the reasons detailed previously (on the basis of the shapes and energies of the frontier orbitals),[39] the $[Cp_2TiMe]^+$ fragment of **12** is more easily distorted (ΔE_{def}(Ti) = 74.0 kJ mol^{-1}) than $[Ti(NMe)(H_3[9]aneN_3)Me]^+$ (ΔE_{def}(Ti) = 87.6 kJ mol^{-1}) leading to **7q**. Considering the actual steric bulk in **7Q** renders the distortion of the methyl cation even more energetically demanding (ΔE_{def}(Ti) = 109.3 kJ mol^{-1}). For the $AlMe_3$ fragment, the deformation energy ΔE_{def}(X) is highest for **12** because the Al−C bonds become significantly longer (ΔE_{def}(X) values: 113.9 kJ mol^{-1} for **12**; 96.4 kJ mol^{-1} for **7q**; 96.3 kJ mol^{-1} for **7Q**). Interestingly, the fragment interaction energy ΔE_{int}(Ti···X) for these three systems are of rather comparable magnitude, with that of **7q** being marginally larger than those for **7Q** and **12**. However, although the formation energies of **7q** and **12** are

Table 4. Formation Energy ΔE (kJ mol^{-1}) of the $AlMe_3$ and $ZnMe_2$ Adducts and Energetic Contribution (kJ mol^{-1}) Defined According to the Thermodynamic Cycle Shown in Figure 5

param	7Q	12	7q	8Q	13	8q	7q′	7Q′
ΔE	−70.4	−88.0	−98.4	−41.3	−56.8	−71.4	−136.1	−68.9
ΔE_{def}(Ti)	109.3	74.0	87.6	76.5	76.0	51.1	53.7	84.4
ΔE_{def}(X)	96.3	113.9	96.4	134.1	118.9	146.5	109.0	123.6
ΔE_{int}(Ti···X)	−276.0	−275.8	−282.5	−251.9	−251.8	−268.9	−298.8	−277.0

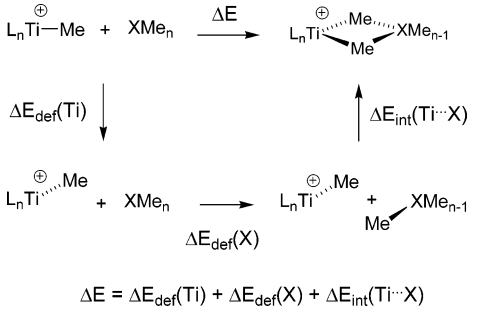

Figure 5. Thermodynamic cycle considered to analyze the formation energy ΔE of the adduct as a sequence of three steps: deformation of the monomethyl cation, ΔE_{def}(Ti); deformation of the XMe_n molecule, ΔE_{def}(X); interaction energy between the two fragments in the geometry of the adduct, ΔE_{int}(Ti···X).

essentially the same, this apparent similarity originates from two different principal causes: an easier to distort [Cp_2TiMe^+] fragment in **12** versus smaller geometric alteration of $AlMe_3$ in **7q**. For **7Q**, increased steric repulsions renders formation of the $AlMe_3$ adduct less energetically favored compared to **12** and **7q** owing to a substantially higher ΔE_{def}(Ti) for [Ti(N^{t}Bu)(Me$_3$[9]aneN$_3$)Me]$^+$ and slightly lower ΔE_{int}(Ti···X) in comparison to **7q**.

The formation energies of the $ZnMe_2$ adducts **8Q**, **8q**, and **13** are ca. 30 kJ mol^{-1} lower than those for the corresponding $AlMe_3$ adducts **7Q**, **7q**, and **12** (Table 4), reflecting an intrinsically diminished tendency to form such species. For the structurally analogous systems **12** and **13**, the deformation of the [$Cp_2TiMe]^+$ and XMe_n moieties are equivalent within ca. 5 kJ mol^{-1} (Table 4). The difference (31.2 kJ mol^{-1}) in formation energy may be traced mainly to a lower interaction energy in **13** (ΔE_{int}(Ti···X) = −251.8 kJ mol^{-1} for **13** and −275.8 kJ mol^{-1} for **12**) as a result of the lower Lewis acidity of Zn compared to Al.

A comparative thermodynamic analysis for the imido-based $ZnMe_2$ adducts **8Q** and **13** is complicated by the different structures of the two systems. The shorter Ti−C(1) distance in **8Q** results in a much lower ΔE_{def}(Ti) (76.5 kJ mol^{-1} for **8Q** vs 109.3 kJ mol^{-1} for **7Q**), but the considerably more distorted $ZnMe_2$ raises ΔE_{def}(X) (134.1 kJ mol^{-1} for **8Q** vs 96.3 kJ mol^{-1} for **7Q**). Since the ΔE_{int}(Ti···X) term for **8Q** is identical to that for **13**, it suggests that the N_{imide}···Zn interaction (N(1)−Zn = 2.296 Å) in **8Q** compensates for the longer Zn−μ-Me distances (2.356 and 2.246 Å in **8Q** vs 2.152 and 2.145 Å in **13**). Indeed, in the order from **8Q** to the smaller model system **8q** (N(1)−Zn = 2.130 Å), the ΔE_{int}(Ti···X) term increases by 17 kJ mol^{-1} in absolute value even though the Zn−μ-Me distances increase to 2.727 and 2.302 Å.

$AlMe_3$ Adducts on Ti=NR? Reduction of the steric bulk in the $ZnMe_2$ adduct **8Q** to give **8q** is accompanied by a stronger N_{imide}···Zn interaction and a ca. −30 kJ mol^{-1} increase of the interaction energy ΔE to −71.4 kJ mol^{-1}, a value virtually identical to that for **7Q**. This outcome, together with our recent

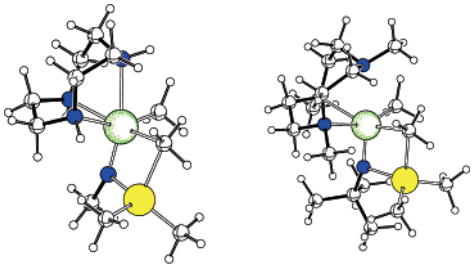

Figure 6. B3PW91-optimized geometry for [Ti(μ-Me)(H$_3$[9]aneN$_3$)(μ-NMe)AlMe$_2$]$^+$ (**7q′**) and [Ti(μ-N^{t}Bu)(Me$_3$[9]aneN$_3$)(μ-Me)AlMe$_2$]$^+$ (**7Q′**).

isolation of the labile N_{imide}···$AlMe_3$ adduct Ti(η-C_8H_8)(μ-N^{t}Bu)(μ-Me)$AlMe_2$ (from the reaction of Ti(η-C_8H_8)(N^{t}Bu) with $AlMe_3$),[76] raises the possibility that certain methyl cations [Ti(NR)(R′$_3$[9]aneN$_3$)Me]$^+$ could alternatively form adducts containing N_{imide}···Al dative interactions. Furthermore, the formation of such adducts in imido-based olefin polymerization catalysts could provide a deactivation pathway that might explain why, in the catalyst systems Ti(NR)(*fac*-N$_3$)Cl$_2$/MAO (R = alkyl or aryl; *fac*-N$_3$ = Me$_3$[9]aneN$_3$[37] or HC(Me$_2$pz)$_3$[38]), only those catalysts with bulky imido R-substituents show significant polymerization activities.

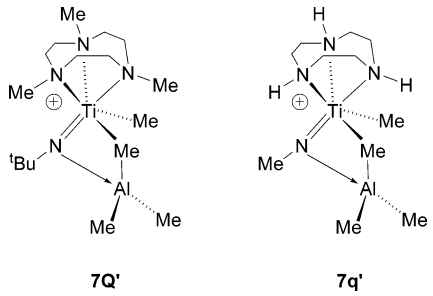

To probe these possibilities, two $AlMe_3$ analogues of **8Q** and **8q** were evaluated by DFT, namely [Ti(μ-N^{t}Bu)(Me$_3$[9]aneN$_3$)Me(μ-Me)$AlMe_2$]$^+$ (**7Q′**) and [Ti(μ-NMe)(H$_3$[9]aneN$_3$)Me(μ-Me)$AlMe_2$]$^+$ (**7q′**). These cations, featuring well-developed N_{imide}···Al interactions, are structural isomers of **7Q** and **7q**, respectively. Geometric parameters are presented in Table 2, thermodynamic parameters pertinent to their formation are listed in Table 4, and geometries are shown in Figure 6.

To separate the electronic and steric effects we first discuss the smaller model system **7q′**. The geometry is best described as an $AlMe_3$ adduct on N, presenting a bridging methyl interaction (C(2)) with Ti. There is a strong interaction with the imido nitrogen atom (Al−N(1) = 2.011 Å) resulting in the disruption of one Ti−N_{imide} π bond (Ti(1)−N(1) = 1.752 Å in **7q′** vs 1.676 Å in **7q**). The bridging methyl is somewhat further

(76) Dunn, S. C.; Hazari, N.; Cowley, A. R.; Green, J. C.; Mountford, P. *Organometallics* **2006**, *25*, 1755.

away from Al in **7q′** than in **7q** (Al−C(2) = 2.136 Å in **7q** and 2.190 Å in **7q′**). This is associated with a concomitant shortening of the Ti−C(2) bond (2.281 Å in **7q** and 2.256 Å in **7q′**). The other titanium methyl group is nonbridging (Ti−C(1) = 2.111 Å, Al−C(1) = 3.967 Å).

The formation energy of **7q′** is 37.8 kJ mol^{-1} more exothermic than that of **7q** ($\Delta E = -98.3$ kJ mol^{-1} for **7q** and −136.1 kJ mol^{-1} for **7q′**), establishing a strong thermodynamic preference for formation of an N_{imide}-bound $AlMe_3$ adduct in the sterically less demanding system. Inevitably, however, formation of this adduct will be critically influenced by the steric bulk at the nitrogen substituent (cf. **8q** vs **8Q**), and in the experimental system $\mathbf{7}^+$, formation of an alternative N_{imide} adduct appears to be inhibited by the imido *tert*-butyl substituent.

The bulkier model system **7Q′** tests this situation. Interestingly, the geometry of the four-membered ring Ti−N(1)−Al−C(2) is not dramatically altered compared to **7q′**; the Ti−N_{imide} bond is only slightly longer (Ti−N(1) = 1.752 Å in **7q′** vs 1.764 Å in **7Q′**), and the Ti−C(2) and Al−C(2) bonds for the bridging methyl do not show significant variations. More remarkably, the Ti−N(1)−C(5) bending angle, a potential reporter of steric bulk at the nitrogen atom, is not indicative of a particular steric pressure at this location of the complex (154.9° in **7q′** vs 156.5° in **7Q′**). The main geometrical change concerns the apical Ti−N bond of the $Me_3[9]aneN_3$ ligand trans to the imido group (2.614 Å in **7Q′** vs 2.370 Å in **7q′**). The introduction of the real ligands in this isomer leads to strong repulsions and, to keep the favorable N_{imide}−Al interaction, results in a loss of bonding for the most weakly bonded ligand, $Me_3[9]aneN_3$. Despite this, formation of this alternative isomer is still predicted to be energetically accessible according to the formation energies ($\Delta E = -68.9$ kJ mol^{-1} for **7Q′** and $\Delta E = -70.4$ kJ mol^{-1} for **7Q**). The experimentally observed system **7Q** is therefore calculated to be marginally more stable (1.5 kJ mol^{-1}) than the nonobserved imido adduct **7Q′**.

The severe destabilization of the N_{imide}−$AlMe_3$ adduct when the steric bulk at the imido ligand is increased is an important result. This causes a reduction in formation energy of 67.2 kJ mol^{-1} on going from **7q′** ($\Delta E = -136.1$ kJ mol^{-1}) to **7Q′** ($\Delta E = -68.9$ kJ mol^{-1}). In contrast, for the (μ-Me)$_2$ dimethyl systems, a loss of formation energy of only ca. 28.2 kJ mol^{-1} is observed on going from **7q** ($\Delta E = -98.4$ kJ mol^{-1}) to **7Q** ($\Delta E = -70.4$ kJ mol^{-1}). This leads to a relative preference for bis(μ-methyl)-bridged dimers over the N_{imide} adducts with $AlMe_3$ when bulky systems are considered. These results are fully consistent with the observed structure−productivity relationships in MAO-catalyed polymerization by the systems Ti(N^tBu)(Me_3-[9]$aneN_3$)Cl_2/MAO.

Conclusions

The reactions of [Ti(N^tBu)($Me_3[9]aneN_3$)Me]$^+$ ($\mathbf{4}^+$) with $AlMe_3$ and $ZnMe_2$, together with DFT investigations of the products and their metallocenium analogues, have allowed a greater understanding of the structures and properties of these key complexes. The results are especially relevant to the academic and commercially important area of olefin polymerization catalysis where these adducts play key roles as intermediates or resting states.

The X-ray crystallographic and/or detailed DFT analyses of [Ti(N^tBu)($Me_3[9]aneN_3$)(μ-Me)$_2$$AlMe_2$]$^+$ ($\mathbf{7}^+$/**7Q**) and [Cp_2Ti-(μ-Me)$_2$$AlMe_2$]$^+$ (**12**) provided new insights into the nature of the bonding and Ti···H−C interactions in the Ti(μ-CH_3)Al bridges of $AlMe_3$ adducts of metal alkyl cations. These are generally contrary to expectations on the basis of the widely studied neutral rare earth systems. Calculations on the less sterically protected model systems [Ti(NMe)($H_3[9]aneN_3$)(μ-Me)$_2$$AlMe_2$]$^+$ (**7q**/**7q′**) found a pronounced electronic preference for strong N_{imide}···$AlMe_3$ coordination. This may help account for the structure−productivity relationships in recently reported imido-supported ethylene polymerization catalyst libraries and helps point toward new approaches to catalyst design in the future.

NMR spectroscopic and/or DFT investigations of the $ZnMe_2$ adducts [Ti(μ-N^tBu)($Me_3[9]aneN_3$)(μ-Me)$_2$ZnMe]$^+$ ($\mathbf{8}^+$/**8Q**) and [Cp_2Ti(μ-Me)$_2$ZnMe]$^+$ (**13**) have provided the first such obervations/analysis of zinc alkyl adducts of transition metal alkyl cations. Experimental and computational evaluations of the relative binding strengths of $AlMe_3$ and $ZnMe_2$ to the respective alkyl cations found $AlMe_3$ to be the better donor. The nature of the bonding and Ti···H−C interactions in the Ti(μ-CH_3)Zn bridges of these bimetallic cations have also been assessed by DFT and compared with those in the $AlMe_3$ adducts. Variable-temperature NMR studies of $\mathbf{8}^+$ found that exchange of all of its metal alkyl groups with those of free $ZnMe_2$ is facile above 253 K, whereas at low temperatures the terminal Zn−Me group of $\mathbf{8}^+$ was able to exchange with those of free $ZnMe_2$ without exchange of the bridging methyls at a comparable rate. These results have significance for chain transfer processes based on added zinc alkyl reagents.

Experimental Section

General Methods and Instrumentation. All manipulations were carried out using standard Schlenk line or drybox techniques under an atmosphere of argon or of dinitrogen. Protio and deutero solvents were predried over activated 4 Å molecular sieves and were refluxed over the appropriate drying agent, distilled, and stored under dinitrogen in Teflon valve ampules. NMR samples were prepared under dinitrogen in 5 mm Wilmad 507-PP tubes fitted with J. Young Teflon valves. ^{1}H, ^{13}C{^{1}H}, ^{19}F, and ^{2}H NMR spectra were recorded on Varian Mercury-VX 300, Varian Unity Plus 500, and Bruker AV500 spectrometers. ^{1}H and ^{13}C assignments were confirmed when necessary with the use of DEPT-135, DEPT-90, and two-dimensional ^{1}H−^{1}H and ^{13}C−^{1}H NMR experiments. ^{1}H and ^{13}C spectra were referenced internally to residual protio solvent (^{1}H) or solvent (^{13}C) resonances and are reported relative to tetramethylsilane ($\delta = 0$ ppm). ^{19}F spectra were referenced externally to $CFCl_3$. Chemical shifts are quoted in δ (ppm), and coupling constants, in hertz. Infrared spectra were prepared as Nujol mulls between NaCl plates and were recorded on a Perkin-Elmer 1710 series FTIR spectrometer. Infrared data are quoted in wavenumbers (cm^{-1}). Mass spectra were recorded by the mass spectrometry service of Oxford University's Department of Chemistry, and elemental analyses, by the analytical services of the University of Oxford Inorganic Chemistry Laboratory or by the Elemental Analysis Service at the London Metropolitan University.

Literature Preparations and Other Starting Materials. The compounds Ti(N^tBu)($Me_3[9]aneN_3$)Me_2 (**3**),[36] Cp_2ZrMe_2,[77] and $Cp_2Zr(CD_3)_2$[56] were prepared according to published methods. [CPh_3][$BAr^F{}_4$] and $BAr^F{}_3$ were kindly provided by DSM Research BV. All other compounds and reagents were purchased and used without further purification.

[Ti(N^tBu)($Me_3[9]aneN_3$)(μ-Me)$_2$$AlMe_2$][$BAr^F{}_4$] (7-$BAr^F{}_4$). To a solution of Ti($N^tBu$)($Me_3[9]aneN_3$)$Me_2$ (0.050 g, 0.156 mmol) and Al_2-

(77) Samuel, E.; Rausch, M. D. *J. Am. Chem. Soc.* **1973**, *95*, 6263.

Me_6 (15.0 μL, 0.078 mmol) in CH_2Cl_2 (2 mL) was added $[CPh_3][BAr^F{}_4]$ (0.144 g, 0.156 mmol) in CH_2Cl_2 (2 mL). The reaction mixture was cooled to 4 °C for 16 h resulting in orange crystals suitable for X-ray diffraction. The mother liquor was carefully decanted away, and the crystals were dried in vacuo. Yield: 0.088 g (53%). ^{1}H NMR (CD_2Cl_2, 500.3 MHz, 293 K): 3.76 (2H, m, CH_2), 3.19 (2H, m, CH_2), 3.18 (6H, s, NMe cis), 2.96 (2H, m, CH_2), 2.84 (2H, m, CH_2), 2.75 (2H, m, CH_2), 2.64 (2H, m, CH_2), 2.34 (3H, s, NMe trans), 1.14 (9H, s, $NCMe_3$), 0.86 (6H, s, μ-$AlMe_2$), −0.48 (3H, s, AlMe "down"), −0.87 (3H, s, AlMe "up"). ^{13}C{^{1}H} NMR (CD_2Cl_2, 125.8 MHz, 293 K): 148.1 (br. d, $^1J_{C-F}$ 243 Hz, 2-C_6F_5), 138.2 (br. d, $^1J_{C-F}$ 243 Hz, 4-C_6F_5), 136.2 (br. d, $^1J_{C-F}$ 243 Hz, 3-C_6F_5), 73.2 ($NCMe_3$), 57.1 (CH_2), 56.6 (CH_2), 55.7 (CH_2), 54.5 (NMe cis), 49.9 (NMe trans), 30.2 ($NCMe_3$), 23.3 (μ-$AlMe_2$), −4.9 (br, AlMe "down"), −7.6 (br., AlMe "up"). ^{19}F NMR (CD_2Cl_2, 282.1 MHz, 293 K): −133.5 (d, ^3J 10.6 Hz, 2-C_6F_5), −164.0 (t, ^3J 20.4 Hz, 4-C_6F_5), −167.9 (app t, app ^3J 18.1 Hz, 3-C_6F_5). IR (NaCl plates, Nujol mull, cm^{-1}): 2922 (s, br.), 2860 (s), 1644 (s), 1515 (s), 1299 (w), 1271 (s), 1233 (s), 1199 (w), 1086 (s), 998 (m), 979 (s), 889 (w), 784 (m), 775 (m), 756 (m), 736 (m), 725 (m), 684 (m), 661 (m). Anal. Found (calcd for $C_{41}H_{42}AlBF_{20}N_4Ti$): C, 46.5 (46.6); H, 3.9 (4.0); N, 5.3 (5.3). "Up" and "down" refer to the orientation with respect to the triazacyclononane ring.

NMR Tube Scale Synthesis of [Ti(μ-N^{t}Bu)(Me_3[9]aneN$_3$)(μ-Me)$_2$ZnMe][B(C_6F_5)$_4$] (8-BAr$^F{}_4$). To a solution of **4**-$BAr^F{}_4$ (generated in situ from Ti(N^{t}Bu)(Me_3[9]aneN$_3$)Me_2 (0.007 g, 0.022 mmol) and $[CPh_3][BAr^F{}_4]$ (0.020 g, 0.022 mmol)) in C_6D_5Cl (0.75 mL) was added a solution of $ZnMe_2$ (2.0 M in toluene, 10.9 μL, 0.022 mmol). After 10 min an ^{1}H NMR spectrum was recorded which showed quantitative conversion to **8**-$BAr^F{}_4$. ^{1}H NMR (C_6D_5Cl, 499.9 MHz, 233 K): 2.79 (2H, m, CH_2), 2.36 (2H, m, CH_2), 2.20 (6H, s, NMe cis), 2.20−2.00 (8H, overlapping m, CH_2), 1.73 (3H, s, NMe trans), 1.05 (9H, s, $NCMe_3$), −0.05 (3H, s, ZnMe), −0.14 (6H, s, μ-$ZnMe_2$). ^{13}C{^{1}H} NMR (C_6D_5Cl, 125.7 MHz, 233 K): 148.5 (br d, $^1J_{C-F}$ 248 Hz, 2-C_6F_5), 138.4 (br d, $^1J_{C-F}$ 238 Hz, 4-C_6F_5), 136.6 (br d, $^1J_{C-F}$ 240 Hz, 3-C_6F_5), 71.0 ($NCMe_3$), 55.3 (CH_2), 55.1 (CH_2), 55.0 (CH_2), 51.6 (NMe cis), 47.6 (NMe trans), 31.4 ($NCMe_3$), 25.7 (μ-$ZnMe_2$), −8.2 (ZnMe). ^{19}F NMR (C_6D_5Cl, 282.1 MHz, 298 K): −132.2 (d, ^3J 12.1 Hz, 2-C_6F_5), −162.3 (t, ^3J 19.6 Hz, 4-C_6F_5), −166.3 (app t, app ^3J 19.6 Hz, 3-C_6F_5).

[Ti(N^{t}Bu){Me_2(μ-CH_2)[9]aneN$_3$}(μ-CH_2)$ZrCp_2$][B(C_6F_5)$_4$] (10-BAr$^F{}_4$). To a solution of Ti(N^{t}Bu)(Me_3[9]aneN$_3$)Me_2 (0.050 g, 0.156 mmol) in C_6H_5Cl (2 mL) was added $[CPh_3][BAr^F{}_4]$ (0.144 g, 0.156 mmol) in C_6H_5Cl (2 mL) to give a bright orange solution. Cp_2ZrMe_2 (0.039 g, 0.156 mmol) in C_6H_5Cl (1 mL) was then added and the solution stirred for 24 h. The solution was concentrated to approximately 1 mL, after which hexane (4 mL) was added with stirring resulting in a deep red oil. The supernatant was decanted and the oil washed with hexane (3 × 2 mL). When a reduced pressure was applied to the oil, an orange powder was obtained. Yield: 0.139 g (74%). The corresponding NMR tube scale reaction of **4**-$MeBAr^F{}_3$ with $Cp_2Zr(CD_3)_2$ in C_6D_5Br showed conversion to **10**-$MeBAr^F{}_3$ after 5 days. Following removal of the volatiles and redissolution in CH_2Cl_2, the ^{2}H NMR spectrum showed no significant resonances apart from those corresponding to some remaining C_6D_5Br. ^{1}H NMR (CD_2Cl_2, 299.9 MHz, 293 K): 6.80 (1H, d, ^2J 10.6 Hz, $TiCH_2Zr$), 6.34 (5H, s, C_5H_5), 6.32 (5H, s, C_5H_5), 5.82 (1H, d, ^2J 10.6 Hz, $TiCH_2Zr$), 3.50−3.20 (4H, overlapping m, NCH_2), 3.09 (3H, s, NMe), 3.05 (1H, d, ^{2}J 9.4 Hz, NCH_2Zr), 3.01−2.42 (8H, overlapping m, NCH_2), 2.35 (3H, s, NMe), 2.28 (1H, d, ^2J 9.4 Hz, NCH_2Zr), 1.23 (9H, s, $NCMe_3$). ^{13}C{^{1}H} NMR (CD_2Cl_2, 75.4 MHz, 293 K): 202.2 ($TiCH_2Zr$), 148.5 (br d, $^1J_{C-F}$ 244 Hz, 2-C_6F_5), 138.6 (br d, $^1J_{C-F}$ 240 Hz, 4-C_6F_5), 136.7 (br d, $^1J_{C-F}$ 249 Hz, 3-C_6F_5), 112.2 (C_5H_5), 112.1 (C_5H_5), 80.2 (NCH_2Zr), 68.8 ($NCMe_3$), 61.7 (NCH_2), 58.2 (NCH_2), 55.6 (NCH_2), 54.6 (NCH_2), 54.5 (NMe), 52.0 (NCH_2), 51.0 (NCH_2), 49.6 (NMe), 34.3 ($NCMe_3$). ^{19}F NMR (CD_2Cl_2, 282.1 MHz, 298 K): −133.5 (d, ^3J 10.6 Hz, 2-C_6F_5), −164.0 (t, ^3J 20.4 Hz, 4-C_6F_5), −167.9 (app t, app ^3J 18.1 Hz, 3-C_6F_5). IR (NaCl plates, Nujol mull, cm^{-1}): 2924 (s), 2854 (s), 1643 (m), 1514 (s), 1275 (m), 1088 (s), 1018 (m), 980 (s), 802 (m), 774 (m), 757 (m), 725 (w), 684 (m), 662 (m). Anal. Found (calcd for $C_{48}H_{41}BF_{20}N_4TiZr$): C, 47.7 (47.9); H, 4.6 (3.4); N, 4.5 (4.7).

Table 5. X-ray Data Collection and Processing Parameters for [Ti(N^{t}Bu)(Me_3[9]aneN$_3$)(μ-$Me)_2AlMe_2$][$BAr^F{}_4$]·CH_2Cl_2 (**7**-$BAr^F{}_4$·CH_2Cl_2)

empirical formula	$C_{41}H_{42}AlBF_{20}N_4Ti\cdot CH_2Cl_2$
fw	1141.40
temp/K	150
wavelength/Å	0.710 73
space group	$P2_1/n$
a/Å	13.7837(2)
b/Å	19.5766(3)
c/Å	18.6673(2)
α/deg	90
β/deg	109.7558(7)
γ/deg	90
V/Å^3	4740.67(11)
Z	4
d(calcd)/Mg·m^{-3}	1.599
abs coeff/mm^{-1}	0.428
R indices [$I > 3\sigma(I)$][a]	
R_1	0.0359
R_w	0.0371

[a] $R_1 = \Sigma||F_o| - |F_c||/\Sigma|F_o|$; $R_w = \sqrt{\{\Sigma w(|F_o| - |F_c|)^2/\Sigma w|F_o|^2\}}$.

Crystal Structure Determination of [Ti(N^{t}Bu)(Me_3[9]aneN$_3$)(μ-$Me)_2$-$AlMe_2$][$BAr^F{}_4$]·CH_2Cl_2 (7-$BAr^F{}_4$·CH_2Cl_2). Crystal data collection and processing parameters are given in Table 5. Crystals were mounted on a glass fiber using perfluoropolyether oil and cooled rapidly to 150 K in a stream of cold N_2 using an Oxford Cryosystems CRYOSTREAM unit. Diffraction data were measured using an Enraf-Nonius KappaCCD diffractometer. Intensity data were processed using the DENZO-SMN package.[78] The structures were solved using the direct-methods program SIR92,[79] which located all non-hydrogen atoms. Subsequent full-matrix least-squares refinement was carried out using the CRYSTALS program suite.[80] Coordinates and anisotropic thermal parameters of all non-hydrogen atoms were refined. Disorder of the CH_2Cl_2 molecule was satisfactorily modeled. Hydrogen atoms were positioned geometrically with the exception of the hydrogen atoms of the metal-bound methyl groups which were located from difference Fourier maps and their coordinates and isotropic thermal parameters subsequently refined. Full listings of atomic coordinates, bond lengths and angles, and displacement parameters have been deposited at the Cambridge Crystallographic Data Center. See Notice to Authors, Issue No. 1.

Computational Details. All the calculations have been performed with the Gaussian03 package[81] at the B3PW91 level.[82,83] The titanium atom was represented by the relativistic effective core potential (RECP) from the Stuttgart group (12 valence electrons) and its associated basis set,[84] augmented by an f polarization function ($\alpha = 0.869$).[85] The Zn atom was represented by RECP from the Stuttgart group and the associated basis set,[86] augmented by a d polarization function.[87] The remaining atoms (C, H, N, Al) were represented by a 6-31G(d,p) basis

(78) Otwinowski, Z.; Minor, W. *Processing of X-ray Diffraction Data Collected in Oscillation Mode*; Academic Press: New York, 1997.
(79) Altomare, A.; Cascarano, G.; Giacovazzo, G.; Guagliardi, A.; Burla, M. C.; Polidori, G.; Camalli, M. *J. Appl. Crystallogr.* **1994**, *27*, 435.
(80) Betteridge, P. W.; Cooper, J. R.; Cooper, R. I.; Prout, K.; Watkin, D. J. *J. Appl. Crystallogr.* **2003**, *36*, 1487.
(81) Pople, J. A.; et al. *Gaussian 03*, revision C.02; Gaussian, Inc.: Wallingford, CT, 2004.
(82) Becke, A. D. *J. Chem. Phys.* **1993**, *98*, 5648.
(83) Perdew, J. P.; Wang, Y. *Phys. Rev. B* **1992**, *45*, 13244.
(84) Andrae, D.; Haussermann, U.; Dolg, M.; Stoll, H.; Preuss, H. *Theor. Chim. Acta* **1990**, *77*, 123.
(85) Ehlers, A. W.; Bohme, M.; Dapprich, S.; Gobbi, A.; Hollwarth, A.; Jonas, V.; Kohler, K. F.; Stegmann, R.; Veldkamp, A.; Frenking, G. *Chem. Phys. Lett.* **1993**, *208*, 111.
(86) Bergner, A.; Dolg, M.; Kuchle, W.; Stoll, H.; Preuss, H. *Mol. Phys.* **1993**, *30*, 1431.
(87) Hollwarth, A.; Bohme, H.; Dapprich, S.; Ehlers, A. W.; Gobbi, A.; Jonas, V.; Kohler, K. F.; Stagmann, R.; Veldkamp, A.; Frenking, G. *Chem. Phys. Lett.* **1993**, *203*, 237.

set.[88] Full optimizations of geometry without any constraint were performed, followed by analytical computation of the Hessian matrix to confirm the nature of the located extrema as minima on the potential energy surface. Natural bonding orbital analysis[89] was performed with the NBO 5.0 version implemented in Gaussian03.

Acknowledgment. We thank the EPSRC, DSM Research BV, CNRS, Egide, and the British Council for support and Dr. N. H. Rees for help with some of the NMR experiments.

Supporting Information Available: X-ray crystallographic file in CIF format for the structure determination of **7**-$BAr^F_4{\cdot}CH_2Cl_2$, an ^1H NMR spectrum of $[Ti(N^tBu)(Me_3[9]aneN_3)(\mu\text{-}Me)_2AlMe_2]^+$ ($\mathbf{7}^+$) at room temperature, ^1H NMR spectra of the cation $[Ti(\mu\text{-}N^tBu)(Me_3[9]aneN_3)(\mu\text{-}Me)_2ZnMe]^+$ ($\mathbf{8}^+$) at different temperatures, with and without added $ZnMe_2$, a complete reference for Gaussian 03- and DFT-computed Cartesian coordinates for the optimized molecules and their electronic energies, and further discussion of the bridging methyl groups (bridging methyl group geometries) and electronic structures of the adducts (Ti···H−C interactions). This material is available free of charge via the Internet at http://pubs.acs.org.

JA065638A

(88) Hariharan, P. C.; Pople, J. A. *Theor. Chim. Acta* **1973**, *28*, 213.

(89) Reed, A. E.; Curtiss, L. A.; Weinhold, F. *Chem. Rev.* **1988**, *88*, 899.